Appendix A

Formulation

A.1 The governing equations for compressible reacting flows

The govering equations used for the simulation in this study have been derived before and used extensively (*e.g.*, Williams, 1985; Buckmaster & Ludford, 1982). However, for completeness, we will review those equations and the difficulties they pose to the numerical study.

First the compressible Navier-Stokes equations will be reviewed, and then several different sets of equations under different levels of assumptions will be derived.

$$\frac{\partial \rho}{\partial t} + \nabla \cdot (\rho \mathbf{u}) = 0, \tag{A.1a}$$

$$\frac{\partial \rho \mathbf{u}}{\partial t} + \nabla \cdot (\rho \mathbf{u}\mathbf{u} - \mathbf{T}) = \rho \mathbf{f}, \tag{A.1b}$$

$$\frac{\partial \rho e_T}{\partial t} + \nabla \cdot (\rho \mathbf{u} e_T - \mathbf{u} \cdot \mathbf{T} + \mathbf{q}) = \rho \mathbf{f} \cdot \mathbf{u} \tag{A.1c}$$

$$\frac{\partial \rho Y_{\mathfrak{m}}}{\partial t} + \nabla \cdot (\rho Y_{\mathfrak{m}} (\mathbf{u} + \mathbf{V}_{\mathfrak{m}})) = \dot{\rho_{\mathfrak{m}}}, \tag{A.1d}$$

where $\mathbf{q}$ is heat flux given by

$$\mathbf{q} = -\lambda_T \nabla T + \rho \sum_{\mathfrak{m}} h_{\mathfrak{m}} Y_{\mathfrak{m}} \mathbf{V}_{\mathfrak{m}} + R_{\mathrm{u}} T \sum_{\mathfrak{m}} \sum_{\mathfrak{n}} \left(\frac{X_{\mathfrak{n}} D_{T,\mathfrak{m}}}{W_{\mathfrak{m}} D_{\mathfrak{m}\mathfrak{n}}} \right) (\mathbf{V}_{\mathfrak{m}} - \mathbf{V}_{\mathfrak{n}}) + \mathbf{q}_R, \tag{A.2}$$

where λ_T is the thermal conductivity, $h_{\mathfrak{m}}$ is the specific enthalpy of species $\mathfrak{m}$, $\mathbf{V}_{\mathfrak{m}}$ is the diffusion velocity for species $\mathfrak{m}$, R_{u} is the universal gas constant, $D_{T,\mathfrak{m}}$ is the thermal diffusion coefficient for species $\mathfrak{m}$, $W_{\mathfrak{m}}$ is molecular weight of species $\mathfrak{m}$, $D_{\mathfrak{m}\mathfrak{n}}$ is binary diffusion

coefficient for species $\mathfrak{m}$ and $\mathfrak{n}$, and $\mathbf{q}_R$ is the radiant heat flux vector.

The stress tensor $\mathbf{T}$ is given by

$$\mathbf{T} = -p\mathbf{I} + \mu\left((\nabla\mathbf{u}) + (\nabla\mathbf{u})^t\right) + \lambda(\nabla\cdot\mathbf{u})\mathbf{I}. \tag{A.3}$$

$\mathbf{V}_\mathfrak{m}$ may be approximated by (Curtiss & Bird, 1999; Bird *et al.*, 2002),

$$\mathbf{V}_\mathfrak{m} = -\frac{D_\mathfrak{m}^T}{T}\nabla T - \sum_\mathfrak{n} D_{\mathfrak{m}\mathfrak{n}}\mathbf{d}_\mathfrak{n} \tag{A.4}$$

where $\mathbf{d}_\mathfrak{n}$ is the diffusion driving force given by,

$$\mathbf{d}_\mathfrak{n} = \nabla X_\mathfrak{n} - (Y_\mathfrak{m} - X_\mathfrak{m})\frac{\nabla p}{p}. \tag{A.5}$$

The first term in Eqn. (A.4) is called Soret effect, which is an effect of thermal diffusion. The species diffusion velocity combines concentration diffusion and pressure diffusion effects, both of which are described in the diffusion driving force.

In these equations, and throughout the thesis, ρ is reserved for density, $\mathbf{u}$ for the velocity vector, e_T for the total energy, $Y_\mathfrak{m}$ for the mass fraction of species $\mathfrak{m}$, and $X_\mathfrak{m}$ for the mole fraction of species $\mathfrak{m}$.

For the transport properties, μ denotes the dynamic viscosity, λ denotes the second coefficient of viscosity, which is equal to $\mu_\mathrm{B} - 2/3\mu$, where μ_B is the bulk viscosity. λ_T denotes the thermal conductivity, $D_{\mathfrak{m}\mathfrak{n}}$ denotes the binary diffusion coefficient between species $\mathfrak{m}$ and $\mathfrak{n}$, and $D_{T,\mathfrak{m}}$ denotes the thermal diffusion coefficient as already defined.

A.1.1 Derivation of other forms of the energy equation

First, we derive several forms of the energy transport equation.

We start with the total energy conservation equation,

$$\frac{\partial\rho e_T}{\partial t} + \nabla\cdot(\rho\mathbf{u}e_T - \mathbf{u}\cdot\mathbf{T} + \mathbf{q}) = \rho\mathbf{f}\cdot\mathbf{u}. \tag{A.6}$$

We then use the momentum equation to obtain the transport equation for the internal energy,

$$\rho\frac{De}{Dt} = \mathbf{T} : \nabla\mathbf{u} - \nabla\cdot\mathbf{q}. \tag{A.7}$$

We then use

$$e = h - p/\rho \tag{A.8}$$

to get the enthalpy transport equation,

$$\rho \frac{Dh}{Dt} = \frac{Dp}{Dt} + \mathbf{\Sigma} : \nabla \mathbf{u} - \nabla \cdot \mathbf{q}, \tag{A.9}$$

where $\mathbf{\Sigma} = 2\mu \mathbf{S} + \lambda(\nabla \cdot \mathbf{u})\mathbf{I}$ is the viscous stress tensor. Eqns. (A.6), (A.7), and (A.9) are equivalent, and there are no additional assumptions in deriving one from another. The enthalpy of the mixture is given by,

$$h = \sum_{\mathfrak{m} \in \mathcal{M}} h_{\mathfrak{m}} Y_{\mathfrak{m}}, \tag{A.10}$$

where,

$$h_{\mathfrak{m}}(T) = h_{\mathfrak{m}}^{0,T_{\text{ref}}} + \int_{T_{\text{ref}}}^{T} C_{p,\mathfrak{m}}(T')dT'. \tag{A.11}$$

Eqn.(A.9) can be written in terms of the temperature evolution as follows:

$$\rho C_{p,\text{mix}} \frac{DT}{Dt} = \frac{Dp}{Dt} + \mathbf{\Sigma} : \nabla \mathbf{u} - \nabla \cdot \mathbf{q} + \sum_{\mathfrak{m}} \nabla \cdot (\rho h_{\mathfrak{m}} Y_{\mathfrak{m}} \mathbf{V}_{\mathfrak{m}}) - \sum_{\mathfrak{m}} \rho Y_{\mathfrak{m}} \mathbf{V}_{\mathfrak{m}} \cdot \nabla h_{\mathfrak{m}} - \sum_{\mathfrak{m}} h_{\mathfrak{m}} \dot{\rho_{\mathfrak{m}}}. \tag{A.12}$$

This form of the energy equation is used later to obtain the low Mach number limit of the energy equation.

A.2 The governing equations in the low Mach number limit

A.2.1 The momentum equation

Following Majda & Sethian (1985) and McMurtry *et al.* (1986), we derive the low Mach number limit of the Navier-Stokes equations with a special consideration to bulk viscosity. First we nondimensionalize the equations:

$$\frac{\partial \rho \mathbf{u}}{\partial t} + \nabla \cdot \left(\rho \mathbf{u}\mathbf{u} + p\mathbf{I} - \mu \left[(\nabla \mathbf{u}) + (\nabla \mathbf{u})^t \right] - \lambda (\nabla \cdot \mathbf{u}) \mathbf{I} \right) = \rho \mathbf{f}. \tag{A.13}$$

Here, μ is the dynamic viscosity and λ is the second coefficient of viscosity, which is related to the bulk viscosity by $\mu_{\text{B}} = \lambda + 2/3\mu$.

We scale the primary variables: $\hat{\rho} = \rho/\rho_0$, $\hat{\mathbf{u}} = \mathbf{u}/u_0$, $\hat{x} = x/x_0$, $\hat{t} = t/t_0$ where $t_0 = x_0/u_0$, $\hat{p} = p/p_0$, and $\hat{\mathbf{f}} = \mathbf{f}/({u_0}^2/x_0)$. Furthermore, define ${c_0}^2 = p_0/\rho_0$, $\hat{\mu} = \mu/\mu_0$, $\hat{\lambda} = \lambda/\mu_0$, $M = u_0/c_0$ and $Re = \rho_0 u_0 x_0/\mu_0$. The subscript 0 denotes the reference values of the corresponding variables which are constants. M denotes the Mach number (Ma is researved for the Markstein number in this study.)

$$\frac{\partial \hat{\rho}\hat{\mathbf{u}}}{\partial \hat{t}} + \hat{\nabla}\cdot\left(\hat{\rho}\hat{\mathbf{u}}\hat{\mathbf{u}} + \frac{1}{M^2}\hat{p}\mathbf{I} - \frac{1}{Re}\left(\hat{\mu}\left[(\hat{\nabla}\hat{\mathbf{u}}) + (\hat{\nabla}\hat{\mathbf{u}})^t\right] - \hat{\lambda}(\hat{\nabla}\cdot\hat{\mathbf{u}})\mathbf{I}\right)\right) = \hat{\rho}\hat{\mathbf{f}}. \tag{A.14}$$

When the external force is gravity, *i.e.*, $\mathbf{f} = -g\mathbf{e}_z$, the RHS becomes $-\hat{\rho}/Fr\,\mathbf{e}_z$, where Fr is the Froude number.

Now we perform an asymptotic expansion for small Mach number. Let ϵ be a small parameter:

$$\hat{p}(\hat{x},\hat{t}) = \hat{p}^0(\hat{x},\hat{t}) + \epsilon\hat{p}^1(\hat{x},\hat{t}) + O(\epsilon^2) \tag{A.15a}$$

$$\hat{\mathbf{u}}(\hat{x},\hat{t}) = \hat{\mathbf{u}}^0(\hat{x},\hat{t}) + \epsilon\hat{\mathbf{u}}^1(\hat{x},\hat{t}) + O(\epsilon^2) \tag{A.15b}$$

$$\hat{\rho}(\hat{x},\hat{t}) = \hat{\rho}^0(\hat{x},\hat{t}) + \epsilon\hat{\rho}^1(\hat{x},\hat{t}) + O(\epsilon^2) \tag{A.15c}$$

$$\hat{\mu}(\hat{x},\hat{t}) = \hat{\mu}^0(\hat{x},\hat{t}) + \epsilon\hat{\mu}^1(\hat{x},\hat{t}) + O(\epsilon^2) \tag{A.15d}$$

$$\hat{\lambda}(\hat{x},\hat{t}) = \hat{\lambda}^0(\hat{x},\hat{t}) + \epsilon\hat{\lambda}^1(\hat{x},\hat{t}) + O(\epsilon^2) \tag{A.15e}$$

and substitute these into Eqn.(A.14). We obtain

$$\begin{aligned}&\frac{1}{M^2}\hat{\nabla}\left(\hat{p}^0 + \epsilon\hat{p}^1 + O(\epsilon^2)\right) = \\ &-\frac{\partial \hat{\rho}^0\hat{\mathbf{u}}^0}{\partial \hat{t}} - \hat{\nabla}\cdot\left(\hat{\rho}^0\hat{\mathbf{u}}^0\hat{\mathbf{u}}^0 - \frac{1}{Re}\left(\hat{\mu}^0\left[(\hat{\nabla}\hat{\mathbf{u}}^0) + (\hat{\nabla}\hat{\mathbf{u}}^0)^t\right] - \hat{\lambda}^0(\hat{\nabla}\cdot\hat{\mathbf{u}}^0)\mathbf{I}\right)\right) + \hat{\rho}^0\hat{\mathbf{f}}^0 + O(\epsilon).\end{aligned} \tag{A.16}$$

The leading order of the RHS are the $O(1)$ terms. If $\hat{p}^0$ balances with this, $M \sim 1$ and we simply obtain the original compressible Navier-Stokes equation. If $\hat{p}^1$ balances with the RHS, $M = O(\epsilon^{1/2})$ and $\nabla\hat{p}^0 = 0$ must hold, which dictates that the leading order pressure term is uniform and a function only of time. For external flow, which is the subject of the current study, we assume that the ambient pressure is constant, thus $\hat{p}^0$ is constant and unity for the present study. However, for internal flows, such as reacting flows in an internal

combustion engine, this term can vary with time.

The O(ϵ) equation leads to the low Mach number equations that are used in the present study,

$$\nabla\hat{p}^1 = -\frac{\partial\hat{\rho}^0\hat{\mathbf{u}}^0}{\partial\hat{t}} - \hat{\nabla}\cdot\left(\hat{\rho}^0\hat{\mathbf{u}}^0\hat{\mathbf{u}}^0 - \frac{1}{Re}\left(\hat{\mu}^0\left[(\hat{\nabla}\hat{\mathbf{u}}^0) + (\hat{\nabla}\hat{\mathbf{u}}^0)^t\right] - \hat{\lambda}^0(\hat{\nabla}\cdot\hat{\mathbf{u}}^0)\mathbf{I}\right)\right) + \hat{\rho}^0\hat{\mathbf{f}}^0. \quad \text{(A.17)}$$

This equation is, in dimensional form,

$$\frac{\partial\rho\mathbf{u}}{\partial t} + \nabla\cdot\left(\rho\mathbf{u}\mathbf{u} + (p(x,t) - p_0)\,\mathbf{I} - \mu\left[(\nabla\mathbf{u}) + (\nabla\mathbf{u})^t\right] - \lambda(\nabla\cdot\mathbf{u})\mathbf{I}\right) = \rho\mathbf{f}. \quad \text{(A.18)}$$

Eqn.(A.18) can also be written as follows:

$$\frac{\partial\rho\mathbf{u}}{\partial t} + \nabla\cdot\left(\rho\mathbf{u}\mathbf{u} + p^*\mathbf{I} - \mu\left[(\nabla\mathbf{u}) + (\nabla\mathbf{u})^t\right]\right) = \rho\mathbf{f}, \quad \text{(A.19)}$$

where

$$p^* = (p(x,t) - p_0) - \left(\mu_{\mathrm{B}} - \frac{2}{3}\mu\right)(\nabla\cdot\mathbf{u}). \quad \text{(A.20)}$$

The bulk viscosity is now combined with the purturbational part of the pressure field.

A.2.2 The equation of state

The equation of state is

$$p = \rho\bar{R}_{\mathrm{gas}}T. \quad \text{(A.21)}$$

We normalize this equation as before and we obtain

$$\hat{p} = \hat{\rho}\hat{T} \quad \text{(A.22)}$$

where $\hat{T} = T/T_0$ and $T_0 = p_0/\rho_0\bar{R}_{\mathrm{gas}}$. Again, using the asymptotic expansion, we obtain the equation of state in the low Mach number limit.

$$\hat{p}^0 = \hat{\rho}^0\hat{T}^0. \quad \text{(A.23)}$$

Note that $\hat{T}^0$ is defined as $\hat{T}(\hat{x},\hat{t}) = \hat{T}^0(\hat{x},\hat{t}) + \epsilon\hat{T}^1(\hat{x},\hat{t}) + O(\epsilon^2)$

The LHS of the equation is constant, and thus this equation relates density and temperature, and they cannot vary independently.

Also note that the reference states satisfy the equation of state, $p_0 = \rho_0 \bar{R}_{\text{gas}} T_0$.

A.2.3 The energy equation

Starting from the temperature transport equation,

$$\rho C_{p,\text{mix}} \frac{DT}{Dt} = \frac{Dp}{Dt} + \boldsymbol{\Sigma} : \nabla \mathbf{u} - \nabla \cdot \mathbf{q} + \sum_{\mathfrak{m}} \nabla \cdot (\rho h_{\mathfrak{m}} Y_{\mathfrak{m}} \mathbf{V}_{\mathfrak{m}}) - \sum_{\mathfrak{m}} \rho Y_{\mathfrak{m}} \mathbf{V}_{\mathfrak{m}} \cdot \nabla h_{\mathfrak{m}} - \sum_{\mathfrak{m}} h_{\mathfrak{m}} \dot{\rho_{\mathfrak{m}}}. \tag{A.24}$$

In a similar way to the momentum equations, we obtain the following leading-order equations.

$$\begin{aligned} \hat{\rho} \hat{C}_{p,\text{mix}} \frac{D\hat{T}}{D\hat{t}} = \frac{D\hat{p}}{D\hat{t}} + \frac{M^2}{Re} \hat{\sigma} : (\hat{\nabla} \hat{\mathbf{u}}) - \frac{1}{RePr} \hat{\nabla} \cdot \hat{\mathbf{q}} \\ + \sum_{\mathfrak{m}} \hat{\nabla} \cdot \left(\hat{\rho} \hat{h_{\mathfrak{m}}} Y_{\mathfrak{m}} \hat{\mathbf{V}}_{\mathfrak{m}} \right) - \sum_{\mathfrak{m}} \hat{\rho} Y_{\mathfrak{m}} \hat{\mathbf{V}}_{\mathfrak{m}} \cdot \hat{\nabla} \hat{h_{\mathfrak{m}}} - \sum_{\mathfrak{m}} \hat{h_{\mathfrak{m}}} \dot{\rho_{\mathfrak{m}}}. \end{aligned} \tag{A.25}$$

Here we defined $Pr = \mu_0 C_{p,\text{mix}_0} / \lambda_{T0}$, $\hat{\lambda_T} = \lambda_T / \lambda_{T0}$, and $C_{p,\text{mix}_0} = \bar{R}_{\text{gas}}$.

Again in the low Mach number limit, the leading order equation becomes

$$\hat{\rho}^0 \hat{C}^{\,0}_{p,\text{mix}} \frac{D\hat{T}^0}{D\hat{t}} = \frac{\partial \hat{p}^0}{\partial t} - \frac{1}{RePr} \hat{\nabla} \cdot \hat{\mathbf{q}}^0 + \sum_{\mathfrak{m}} \hat{\nabla} \cdot \left(\hat{\rho}^0 \hat{h_{\mathfrak{m}}}^{\,0} Y^0_{\mathfrak{m}} \hat{\mathbf{V}}_{\mathfrak{m}}^{\,0} \right) - \sum_{\mathfrak{m}} \hat{\rho}^0 Y^0_{\mathfrak{m}} \hat{\mathbf{V}}_{\mathfrak{m}}^{\,0} \cdot \hat{\nabla} \hat{h_{\mathfrak{m}}}^{\,0} - \sum_{\mathfrak{m}} \hat{h_{\mathfrak{m}}}^{\,0} \dot{\rho_{\mathfrak{m}}}. \tag{A.26}$$

The first term on the RHS drops for external flow where ambient pressure is constant in time.

A.2.4 Species transport equations

The species transport equation, Eqn. A.1d, does not change its form at the low Mach number limit. However, in the low Mach number limit, the pressure diffusion term in Eqn.(A.5) is dropped from the leading-order balance for the diffusion velocity. Further, if the thermal diffusion (Soret effect) is negligible, we can use a Fickian diffusion model:

$$Y_{\mathfrak{m}} \mathbf{V}_{\mathfrak{m}} = -D_{\mathfrak{m}} \nabla Y_{\mathfrak{m}}, \tag{A.27}$$

where $D_{\mathfrak{m}}$ is the mixture-averaged diffusion coefficient of species $\mathfrak{m}$.

It should be pointed out that the Soret effect can be of comparable order to the Fickian diffusion term (Ern & Giovangigli, 1998), if included, near the flame front where the

temperature gradient is large (Dimotakis, 2005). Therefore, computed flame thickness may contain some error. However, its influence on flame speed is not significant as shown by Ern & Giovangigli (1999), and the difference was mostly observed in rich flames in their study.

It is known that the inclusion of the Soret effect needs to be accomodated with a change in a wall boundary condition. $\mathbf{V}_\mathrm{m} = 0$ at the boundary does not necessarily translate to $\mathbf{n} \cdot \nabla Y_\mathrm{m} = 0$ on the boundary when additional diffusion terms are included. In particular, when iso-thermal wall boundary condition is used, the boundary conditions to species transport equations must be derived from Eqns. (A.4) and (A.5) to be consistent with a diffusion model.

A.2.5 Transport properties

For viscosity and other transport properties, we know μ and λ, or alternatively $\hat{\mu}$ and $\hat{\lambda}$ as a function of temperature θ. To solve the leading-order momentum equations, we need μ^0 and λ^0 as a function of θ^0. The Taylor series expansion gives us $\hat{\mu}(\hat{\theta}) = \mu^0(\theta^0) + O(\epsilon)$ and $\hat{\lambda}(\hat{\theta}) = \lambda^0(\theta^0) + O(\epsilon)$.

Even when the compositions (Y_ms) change, the same argument follows.

A.3 The governing equations used in this study

The low Mach number equations derived above can be written in the following form for equations in dimensional form:

$$\frac{\partial \rho}{\partial t} + \nabla \cdot (\rho \mathbf{u}) = 0, \tag{A.28a}$$

$$\frac{\partial \mathbf{u}}{\partial t} + \mathbf{u} \cdot \nabla \mathbf{u} = -\frac{1}{\rho} \nabla p^* + \frac{1}{\rho} \nabla \cdot \left(\mu \left[\nabla \mathbf{u} + \nabla \mathbf{u}^t \right] \right) + \mathbf{f}, \tag{A.28b}$$

$$\frac{\partial Y_\mathrm{m}}{\partial t} + \mathbf{u} \cdot \nabla Y_\mathrm{m} = -\frac{1}{\rho} \nabla \cdot (\rho Y_\mathrm{m} \mathbf{V}_\mathrm{m}) + \dot{\omega}_\mathrm{m}, \tag{A.28c}$$

$$\rho C_{p,\mathrm{mix}} \frac{DT}{Dt} = \nabla \cdot (\lambda_T \nabla T) - \rho \sum_\mathrm{m} h_\mathrm{m} \dot{\omega}_\mathrm{m} - \sum_\mathrm{m} \rho Y_\mathrm{m} \mathbf{V}_\mathrm{m} \cdot \nabla h_\mathrm{m}, \tag{A.28d}$$

$$\rho = p_0 / (\bar{R}_\mathrm{gas} T). \tag{A.28e}$$

Expand the viscous term of Eqn.(A.28b) to obtain

$$\frac{\partial \mathbf{u}}{\partial t} + \mathbf{u} \cdot \nabla \mathbf{u} = -\frac{1}{\rho} \nabla p^* + \mathbf{L}^e(\mathbf{u}) + \mathbf{L}^i(\mathbf{u}) + \mathbf{f}, \tag{A.29}$$

where

$$\mathbf{L}^i(\mathbf{u}) = \frac{\mu}{\rho} \nabla^2 \mathbf{u} \tag{A.30a}$$

$$\mathbf{L}^e(\mathbf{u}) = \frac{\mu}{\rho} \nabla \left[\nabla \cdot \mathbf{u} \right] + \frac{\nabla \mu}{\rho} \cdot \left[\nabla \mathbf{u} + \nabla \mathbf{u}^t \right] \tag{A.30b}$$

This particular form of the momentum equation is integrated. One could combine the axial and radial momentum equations to obtain the fully coupled weak formulation of the momentum equations that allows the entire viscous term to be treated implicitly. However, for efficiency reasons, the above approach is taken in this study. The viscous term is further split into the explicit part and the implicit part to save computational time in forming the stiffness matrix used in the implicit integration of the viscous term. Details can be found in Chapter 3.

For the species transport equations, $\mathbf{V}_{\mathfrak{m}}$ needs to be modeled, and the Fickian diffusion model is used in this study.

The diffusion velocity of species $\mathfrak{m}$ must satisfy the following:

$$\sum_{\mathfrak{m}} Y_{\mathfrak{m}} \mathbf{V}_{\mathfrak{m}} = 0. \tag{A.31}$$

This constraint is the result of mass conservation. However, a drawback of using the Fickian diffusion model is that this constraint on $\mathbf{V}_{\mathfrak{m}}$ may not be satisifed. A technique proposed by Coffee & Heimerl (1981) defines a corrective differential velocity, V_c such that

$$\mathbf{V}_c = -\sum_{\mathfrak{m}} Y_{\mathfrak{m}} \tilde{\mathbf{V}}_{\mathfrak{m}}, \tag{A.32}$$

where $\tilde{\mathbf{V}}_{\mathfrak{m}}$ now follows the Fickian model:

$$\tilde{\mathbf{V}}_{\mathfrak{m}} = -\frac{D_{\mathfrak{m}}}{Y_{\mathfrak{m}}} \nabla Y_{\mathfrak{m}}, \tag{A.33}$$

so that

$$\mathbf{V}_{\mathfrak{m}} = \tilde{\mathbf{V}}_{\mathfrak{m}} + \mathbf{V}_c, \tag{A.34}$$

therefore

$$\sum_{\mathfrak{m}} Y_{\mathfrak{m}} \mathbf{V}_{\mathfrak{m}} = 0. \tag{A.35}$$

Effectively, this method subtracts the correct amount of excessive diffusion distributed equally among all species existing in the system. For example, Day & Bell (2000) used this algorithm in their study. However, use of this algorithm in an implicit method is not practical because Eqn.(A.32) couples the entire species through summation. If one of the species is inert and abundant,

$$V_{\mathfrak{m}'} = \frac{1}{Y_{\mathfrak{m}'}} \left(\sum_{\mathfrak{m} \in \mathcal{M}'} D_{\mathfrak{m}} \nabla Y_{\mathfrak{m}} \right), \tag{A.36}$$

where $\mathfrak{m}'$ is the abundant species (nitrogen in this study), and the set $\mathcal{M}'$ contains all the other species but $\mathfrak{m}'$. This is a more practical method to satisfy the constraint without sacrificing efficiency.

Again, similar to the momentum equation, the diffusion term is expanded into an explicit part and an implicit part:

$$\frac{\partial Y_{\mathfrak{m}}}{\partial t} + \mathbf{u} \cdot \nabla Y_{\mathfrak{m}} = D_{\mathfrak{m}} \nabla^2 Y_{\mathfrak{m}} + \frac{1}{\rho} \nabla \rho D_{\mathfrak{m}} \cdot \nabla Y_{\mathfrak{m}} + \dot{\omega}_{\mathfrak{m}} \tag{A.37}$$

for $\mathfrak{m} \in \mathcal{M}'$. It should be noted that as a result of the constraint Eqn.(A.36) and the mass conservation, Y_{N_2} is uniquely determined by the constraint, Eqn.(2.50).

When the Fickian diffusion model is employed, the last term in Eqn.(A.28d) disappears. The radiant heat flux is ignored because it has a noticable effect only at the lean flammability limits (Egolfopoulos, 1994). The Dufour heat flux is also negligible (Ern & Giovangigli, 1998; Williams, 1985). By putting those assumptions into the low Mach number limit of the temperature transport equations, we obtain,

$$\rho C_{p,\mathrm{mix}} \frac{DT}{Dt} = \lambda_T \nabla^2 T + \nabla \lambda_T \cdot \nabla T - \rho \sum_{\mathfrak{m}} h_{\mathfrak{m}} \dot{\omega}_{\mathfrak{m}}. \tag{A.38}$$

Again, the diffusion term has been split into explicit and implicit parts.

A.4 The differential form of the equations in cylindrical coordinates

Vector notation is used throughout this thesis, however, an explicit derivative formulation is necessary to implement the evaluation of derivatives. The differential form of various tensor expressions in cylindrical coordinates can be found in Lagerstrom (1964) and Emmons (1958).

Let (r, θ, z) be the radial, azimuthal, and axial coordinates of the cylindrical polar coordinate respectively, and (u_r, u_θ, u_z) be the corresponding velocity vector. To compute the stress tensor in cylindrical coordinates, we need the following:

$$\nabla \mathbf{u} = \begin{pmatrix} \frac{\partial u_r}{\partial r} & \frac{1}{r}\frac{\partial u_r}{\partial \theta} - \frac{u_\theta}{r} & \frac{\partial u_r}{\partial z} \\ \frac{\partial u_\theta}{\partial r} & \frac{1}{r}\frac{\partial u_\theta}{\partial \theta} + \frac{u_r}{r} & \frac{\partial u_\theta}{\partial z} \\ \frac{\partial u_z}{\partial r} & \frac{1}{r}\frac{\partial u_z}{\partial \theta} & \frac{\partial u_z}{\partial z} \end{pmatrix} \tag{A.39}$$

and let $\mathbf{T}$ be a 3-dimensional tensor of rank 2, then

$$\nabla \cdot \mathbf{T} = \begin{pmatrix} \frac{\partial \tau_{rr}}{\partial r} + \frac{\tau_{rr}}{r} + \frac{1}{r}\frac{\partial \tau_{r\theta}}{\partial \theta} - \frac{\tau_{\theta\theta}}{r} + \frac{\partial \tau_{rz}}{\partial z} \\ \frac{\partial \tau_{\theta r}}{\partial r} + \frac{\tau_{\theta r}}{r} + \frac{1}{r}\frac{\partial \tau_{\theta\theta}}{\partial \theta} + \frac{\tau_{r\theta}}{r} + \frac{\partial \tau_{\theta z}}{\partial z} \\ \frac{\partial \tau_{zr}}{\partial r} + \frac{\tau_{zr}}{r} + \frac{1}{r}\frac{\partial \tau_{z\theta}}{\partial \theta} + \frac{\partial \tau_{zz}}{\partial z} \end{pmatrix}. \tag{A.40}$$

Therefore, the viscous stress tensor, $\mathbf{T} = \mu[(\nabla \mathbf{u}) + (\nabla \mathbf{u})^T]$ has the following form,

$$\mathbf{T} = \begin{pmatrix} 2\mu\frac{\partial u_r}{\partial r} & \mu\left(\frac{1}{r}\frac{\partial u_r}{\partial \theta} - \frac{u_\theta}{r} + \frac{\partial u_\theta}{\partial r}\right) & \mu\left(\frac{\partial u_r}{\partial z} + \frac{\partial u_z}{\partial r}\right) \\ \mu\left(\frac{1}{r}\frac{\partial u_r}{\partial \theta} - \frac{u_\theta}{r} + \frac{\partial u_\theta}{\partial r}\right) & 2\mu\left(\frac{1}{r}\frac{\partial u_\theta}{\partial \theta} + \frac{u_r}{r}\right) & \mu\left(\frac{\partial u_\theta}{\partial z} + \frac{1}{r}\frac{\partial u_z}{\partial \theta}\right) \\ \mu\left(\frac{\partial u_r}{\partial z} + \frac{\partial u_z}{\partial r}\right) & \mu\left(\frac{\partial u_\theta}{\partial z} + \frac{1}{r}\frac{\partial u_z}{\partial \theta}\right) & 2\mu\frac{\partial u_z}{\partial z} \end{pmatrix}. \tag{A.41}$$

So that, the viscous term in the momentum equation is,

$$\nabla \cdot \mathbf{T} = \begin{pmatrix} \frac{1}{r}\frac{\partial}{\partial r}\left(2\mu r \frac{\partial u_r}{\partial r}\right) + \frac{1}{r}\frac{\partial}{\partial \theta}\left(\mu\left(\frac{1}{r}\frac{\partial u_r}{\partial \theta} - \frac{u_\theta}{r} + \frac{\partial u_\theta}{\partial r}\right)\right) - \frac{1}{r}\left(2\mu\left(\frac{1}{r}\frac{\partial u_\theta}{\partial \theta} + \frac{u_r}{r}\right)\right) \\ \qquad\qquad + \frac{\partial}{\partial z}\left(\mu\left(\frac{\partial u_r}{\partial z} + \frac{\partial u_z}{\partial r}\right)\right) \\ \frac{1}{r}\frac{\partial}{\partial r}\left(\mu r\left(\frac{1}{r}\frac{\partial u_r}{\partial \theta} - \frac{u_\theta}{r} + \frac{\partial u_\theta}{\partial r}\right)\right) + \frac{1}{r}\frac{\partial}{\partial \theta}\left(2\mu\left(\frac{1}{r}\frac{\partial u_\theta}{\partial \theta} + \frac{u_r}{r}\right)\right) \\ \qquad\qquad + \frac{1}{r}\left(\mu\left(\frac{1}{r}\frac{\partial u_r}{\partial \theta} - \frac{u_\theta}{r} + \frac{\partial u_\theta}{\partial r}\right)\right) + \frac{\partial}{\partial z}\left(\mu\left(\frac{\partial u_\theta}{\partial z} + \frac{1}{r}\frac{\partial u_z}{\partial \theta}\right)\right) \\ \frac{1}{r}\frac{\partial}{\partial r}\left(\mu r\left(\frac{\partial u_r}{\partial z} + \frac{\partial u_z}{\partial r}\right)\right) + \frac{1}{r}\frac{\partial}{\partial \theta}\left(\mu\left(\frac{\partial u_\theta}{\partial z} + \frac{1}{r}\frac{\partial u_z}{\partial \theta}\right)\right) + \frac{\partial}{\partial z}\left(2\mu\frac{\partial u_z}{\partial z}\right) \end{pmatrix}, \tag{A.42}$$

which is in the case of axisymmetry,

$$\nabla \cdot \mathbf{T} = \begin{pmatrix} \frac{1}{r}\frac{\partial}{\partial r}\left(2\mu r \frac{\partial u_r}{\partial r}\right) - 2\mu\frac{u_r}{r^2} + \frac{\partial}{\partial z}\left(\mu\left(\frac{\partial u_r}{\partial z} + \frac{\partial u_z}{\partial r}\right)\right) \\ 0 \\ \frac{1}{r}\frac{\partial}{\partial r}\left(\mu r\left(\frac{\partial u_r}{\partial z} + \frac{\partial u_z}{\partial r}\right)\right) + \frac{\partial}{\partial z}\left(2\mu\frac{\partial u_z}{\partial z}\right) \end{pmatrix}. \tag{A.43}$$

Similarly, the nonlinear terms in the momentum equations are

$$\mathbf{u} \cdot \nabla \mathbf{u} = \begin{pmatrix} u_r\frac{\partial u_r}{\partial r} + \frac{u_\theta}{r}\frac{\partial u_r}{\partial \theta} - \frac{u_\theta^2}{r} + u_z\frac{\partial u_r}{\partial z} \\ u_r\frac{\partial u_\theta}{\partial r} + \frac{u_\theta}{r}\frac{\partial u_\theta}{\partial \theta} + \frac{u_r u_\theta}{r} + u_z\frac{\partial u_\theta}{\partial z} \\ u_r\frac{\partial u_z}{\partial r} + \frac{u_\theta}{r}\frac{\partial u_z}{\partial \theta} + u_z\frac{\partial u_z}{\partial z} \end{pmatrix}, \tag{A.44}$$

which is in the axisymmetric case,

$$\mathbf{u} \cdot \nabla \mathbf{u} = \begin{pmatrix} u_r\frac{\partial u_r}{\partial r} + u_z\frac{\partial u_r}{\partial z} \\ 0 \\ u_r\frac{\partial u_z}{\partial r} + u_z\frac{\partial u_z}{\partial z} \end{pmatrix}. \tag{A.45}$$

The vector equation (A.28b) is comprised of two equations in differential form,

$$\begin{aligned} \frac{\partial u_z}{\partial t} + \left(u_z\frac{\partial u_z}{\partial z} + u_r\frac{\partial u_z}{\partial r}\right) = &-\frac{1}{\rho}\frac{\partial p^*}{\partial z} \\ &+ \frac{1}{\rho}\left\{\frac{1}{r}\frac{\partial}{\partial r}\left(\mu r\left(\frac{\partial u_r}{\partial z} + \frac{\partial u_z}{\partial r}\right)\right) + \frac{\partial}{\partial z}\left(2\mu\frac{\partial u_z}{\partial z}\right)\right\} + f_z \end{aligned} \tag{A.46}$$

and

$$\frac{\partial u_r}{\partial t} + \left(u_z \frac{\partial u_r}{\partial z} + u_r \frac{\partial u_r}{\partial r} \right) = -\frac{1}{\rho} \frac{\partial p^*}{\partial r} + \frac{1}{\rho} \left\{ \frac{1}{r} \frac{\partial}{\partial r} \left(2\mu r \frac{\partial u_r}{\partial r} \right) - 2\mu \frac{u_r}{r^2} + \frac{\partial}{\partial z} \left(\mu \left(\frac{\partial u_r}{\partial z} + \frac{\partial u_z}{\partial r} \right) \right) \right\} + f_r \tag{A.47}$$

for the cylindrical coordinates when the flow is axisymmetric ($\partial/\partial\theta = 0$) and there is no swirl ($u_\theta = 0$), both of which are assumed in this study.

Appendix B

Initial conditions to unsteady flame simulations

B.1 Introduction

Although the initial conditions to a time-dependent problem are important, not much attention has been paid to this aspect. Unfortunately, many multidimensional numerical studies on reacting flows that employed unsteady equations—Day & Bell (2000); Tomboulides *et al.* (1997); Frouzakis *et al.* (1998)—did not clearly describe the initial condition in their paper. In the present study, a one-dimensional solution using Cantera is used to create an initial condition for the Phase II flame simulation as follows:

$$u(z,r) = f(r;0.00425,0.0025)u^{\text{Cantera}}(z) \tag{B.1a}$$

$$v(z,r) = f(r;0.00425,0.0025)rv^{\text{Cantera}}(z) \tag{B.1b}$$

$$T(z,r) = T^{\text{Cantera}}(z) \tag{B.1c}$$

$$Y_{\mathfrak{m}}(z,r) = f(r;0.005,0.0005)Y_{\mathfrak{m}} \tag{B.1d}$$

$$\tag{B.1e}$$

where $f(r;r_0,\delta r)$ is a blending function that takes a value between 0 and 1, and is defined by

$$f(r;r_0,\delta r) = \left\{\tanh\left[\frac{2.64665}{\delta r/2}(r_0-r)\right]+1\right\}/2 \tag{B.2}$$

where the value of 2.64665 is obtained by $\tanh^{-1}(0.99)$. In other words, r_0 specifies the half-value location, and δr specifies the width of the 99 % window.

In obtaining the one-dimensional solution using Cantera, error torelances and grid refine-

ment parameters are tightened to obtain the numerical solution on a successively increased number of points, starting from around 100. The final solution is solved on more than 1,000 points.

Then, the initial conditions to the Phase III simulations are obtained by combining two different numerical solutions. One is the Phase II solution. The other is the cold flow numerical solution of the nozzle interior flow with the nozzle filled by the mixture at the inflow condition.

B.2 Conversion tables

Throughout this study, air is assumed to be composed of 21% Oxygen and 79% Nitrogen by volume, which is $Y_{\text{oxygen}} = 0.232918$ and $Y_{\text{nitrogen}} = 0.767082$. Table B.1 tabulates mole fractions and mass fractions of Methane, Oxygen, and Nitrogen at various equivalence ratios. Note the equivalence ratios tabulated here are accurate up to the sixth digit, *i.e.*, 1.30 should read 1.300000.

Table B.1: Methane / Air flame equivalence ratio to mass fraction

Φ	X_{CH_4}	X_{O_2}	X_{N_2}	Y_{CH_4}	Y_{O_2}	Y_{N_2}
0.50	0.049881	0.199525	0.750594	0.028366	0.226311	0.745324
0.55	0.054597	0.198535	0.746868	0.031114	0.225671	0.743215
0.60	0.059266	0.197554	0.743180	0.033847	0.225034	0.741119
0.65	0.063890	0.196583	0.739527	0.036564	0.224401	0.739035
0.70	0.068468	0.195622	0.735911	0.039266	0.223772	0.736962
0.75	0.073001	0.194670	0.732329	0.041954	0.223146	0.734901
0.80	0.077491	0.193727	0.728782	0.044626	0.222523	0.732851
0.85	0.081937	0.192793	0.725270	0.047283	0.221905	0.730813
0.90	0.086341	0.191868	0.721791	0.049925	0.221289	0.728786
0.95	0.090702	0.190952	0.718345	0.052553	0.220677	0.726770
1.00	0.095023	0.190045	0.714932	0.055167	0.220068	0.724765
1.05	0.099302	0.189147	0.711551	0.057766	0.219463	0.722772
1.10	0.103541	0.188256	0.708203	0.060350	0.218861	0.720789
1.15	0.107740	0.187375	0.704885	0.062921	0.218262	0.718817
1.20	0.111901	0.186501	0.701599	0.065477	0.217667	0.716856
1.25	0.116022	0.185635	0.698343	0.068020	0.217074	0.714905
1.30	0.120106	0.184778	0.695117	0.070549	0.216485	0.712966
1.35	0.124152	0.183928	0.691920	0.073064	0.215900	0.711036
1.40	0.128160	0.183086	0.688753	0.075566	0.215317	0.709117
1.45	0.132133	0.182252	0.685615	0.078054	0.214737	0.707209
1.50	0.136069	0.181425	0.682505	0.080529	0.214161	0.705310

Appendix C

Flame simulation data

C.1 Phase II: 2D numerical experiments in cylindrical domain

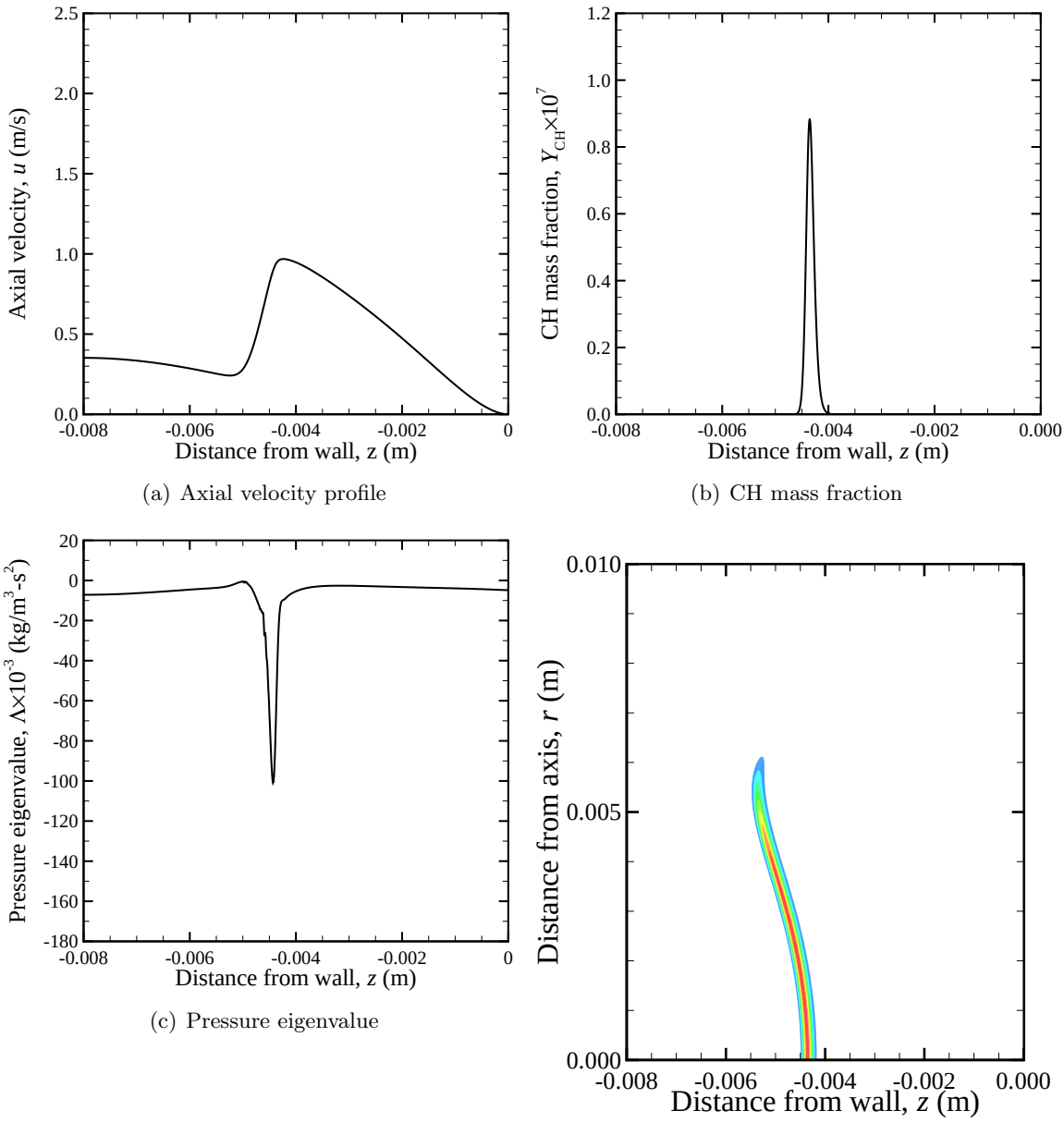

(a) Axial velocity profile

(b) CH mass fraction

(c) Pressure eigenvalue

(d) CH contour

Figure C.1: Φ=0.70, Case B070-2

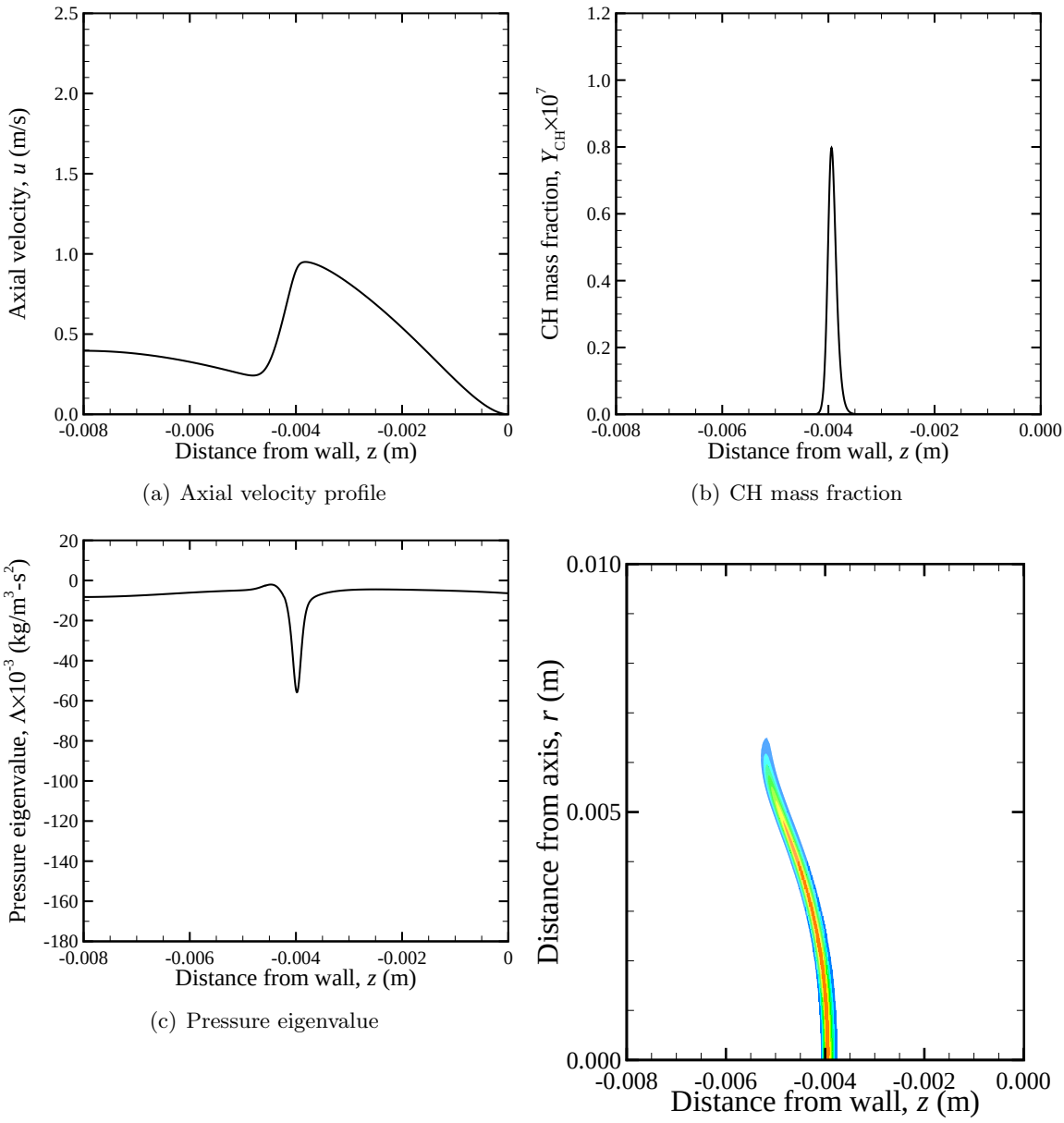

(a) Axial velocity profile

(b) CH mass fraction

(c) Pressure eigenvalue

(d) CH contour

Figure C.2: Φ=0.70, Case B070-7

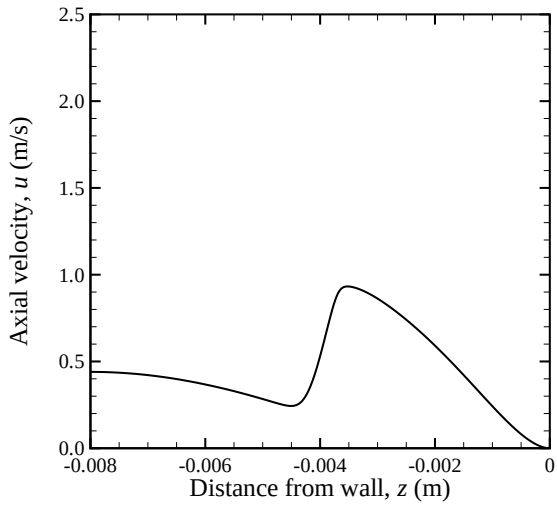

(a) Axial velocity profile

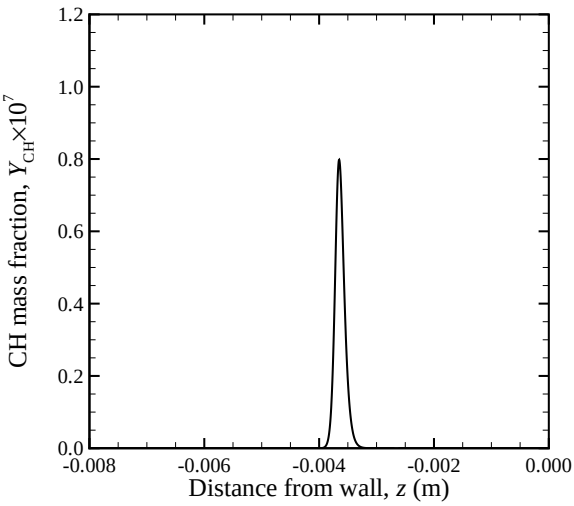

(b) CH mass fraction

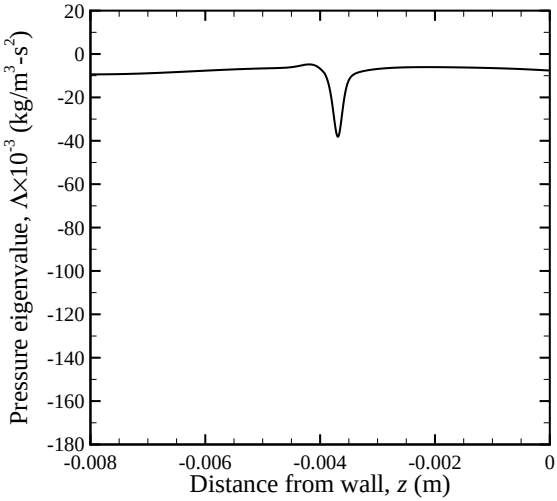

(c) Pressure eigenvalue

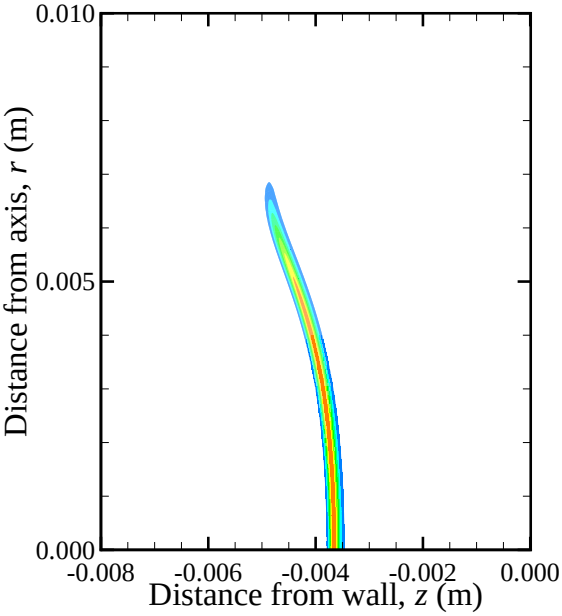

(d) CH contour

Figure C.3: Φ=0.70, Case B070-12

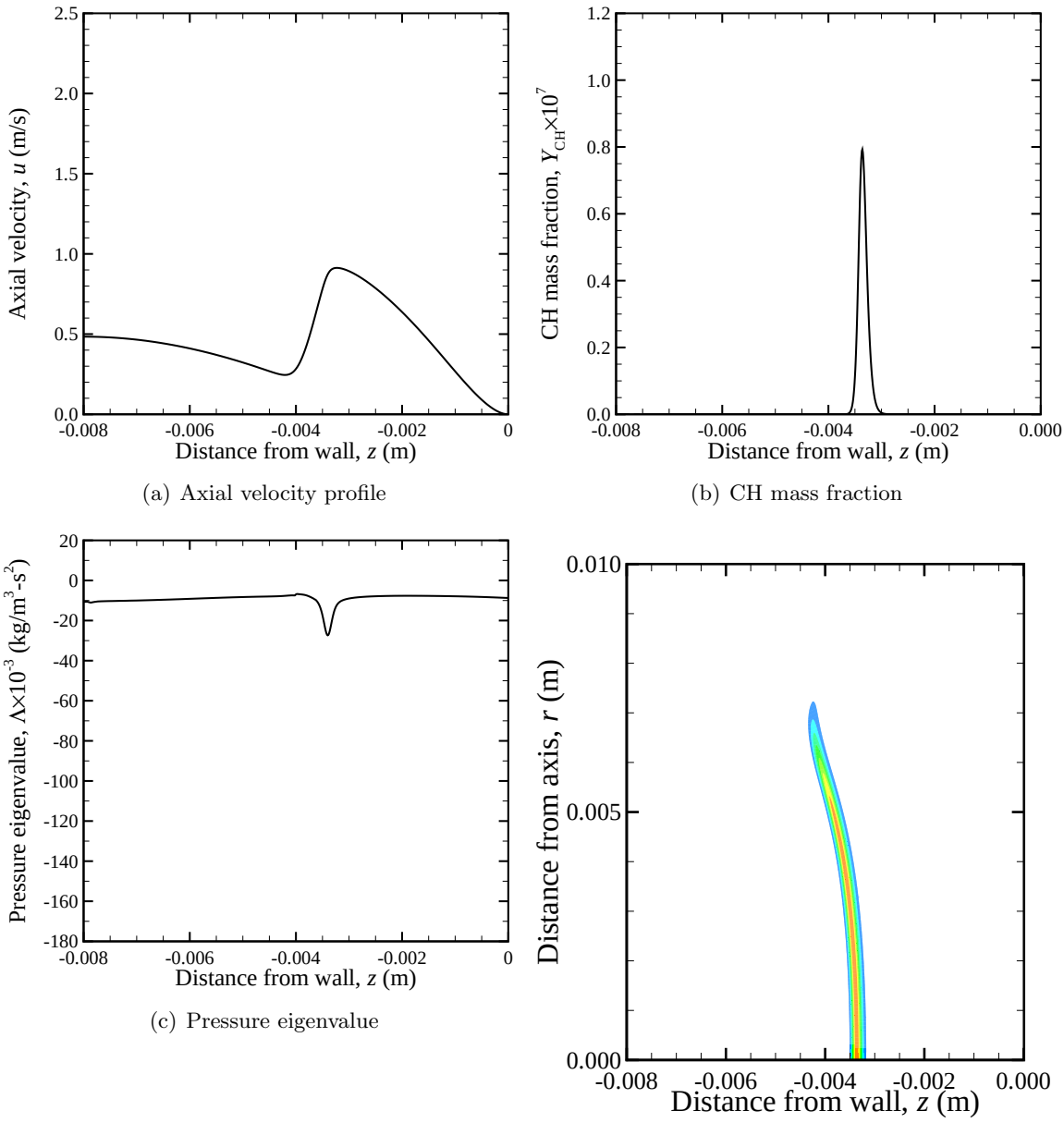

(a) Axial velocity profile

(b) CH mass fraction

(c) Pressure eigenvalue

(d) CH contour

Figure C.4: Φ=0.70, Case B070-17

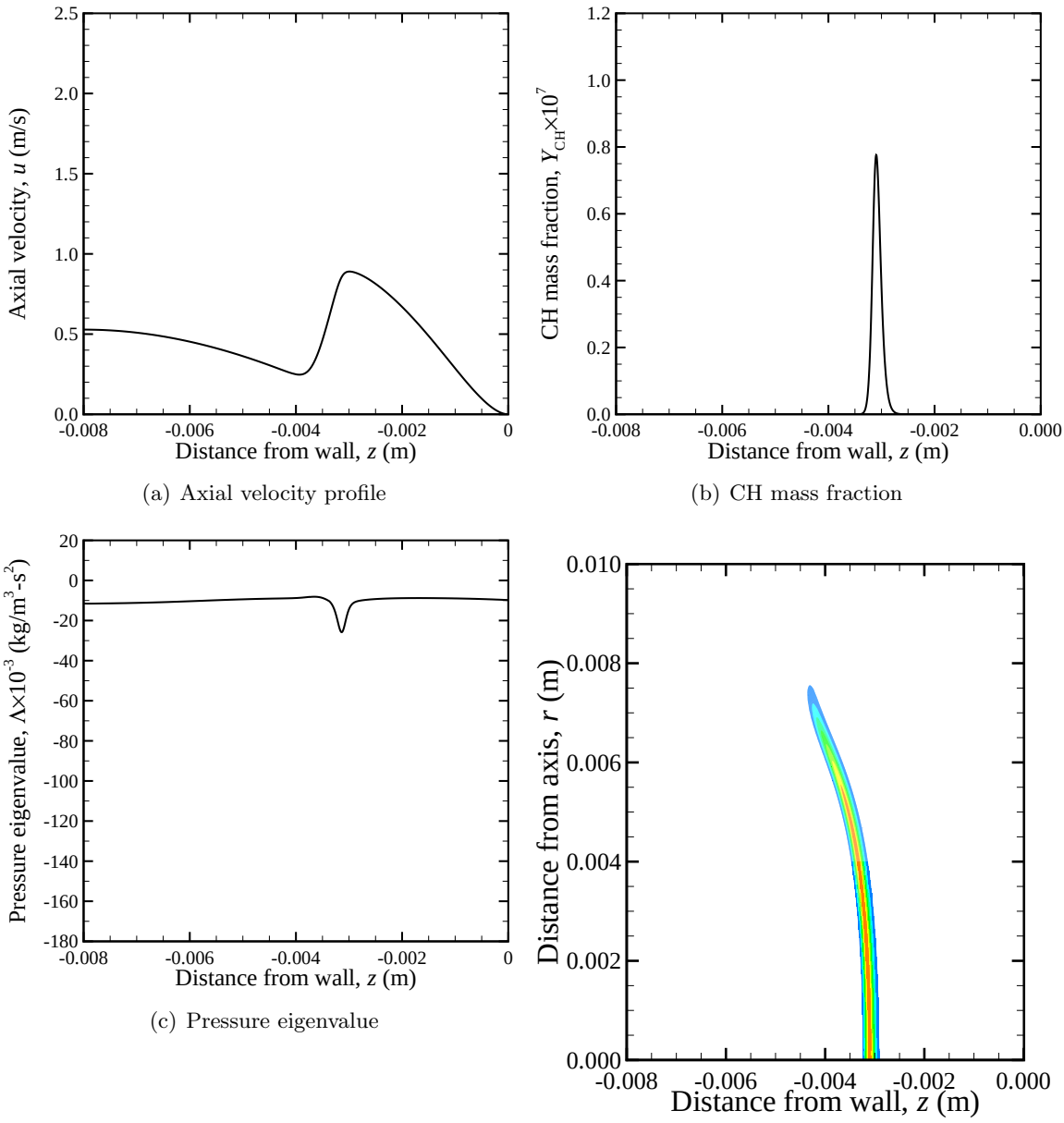

(a) Axial velocity profile

(b) CH mass fraction

(c) Pressure eigenvalue

(d) CH contour

Figure C.5: Φ=0.70, Case B070-22

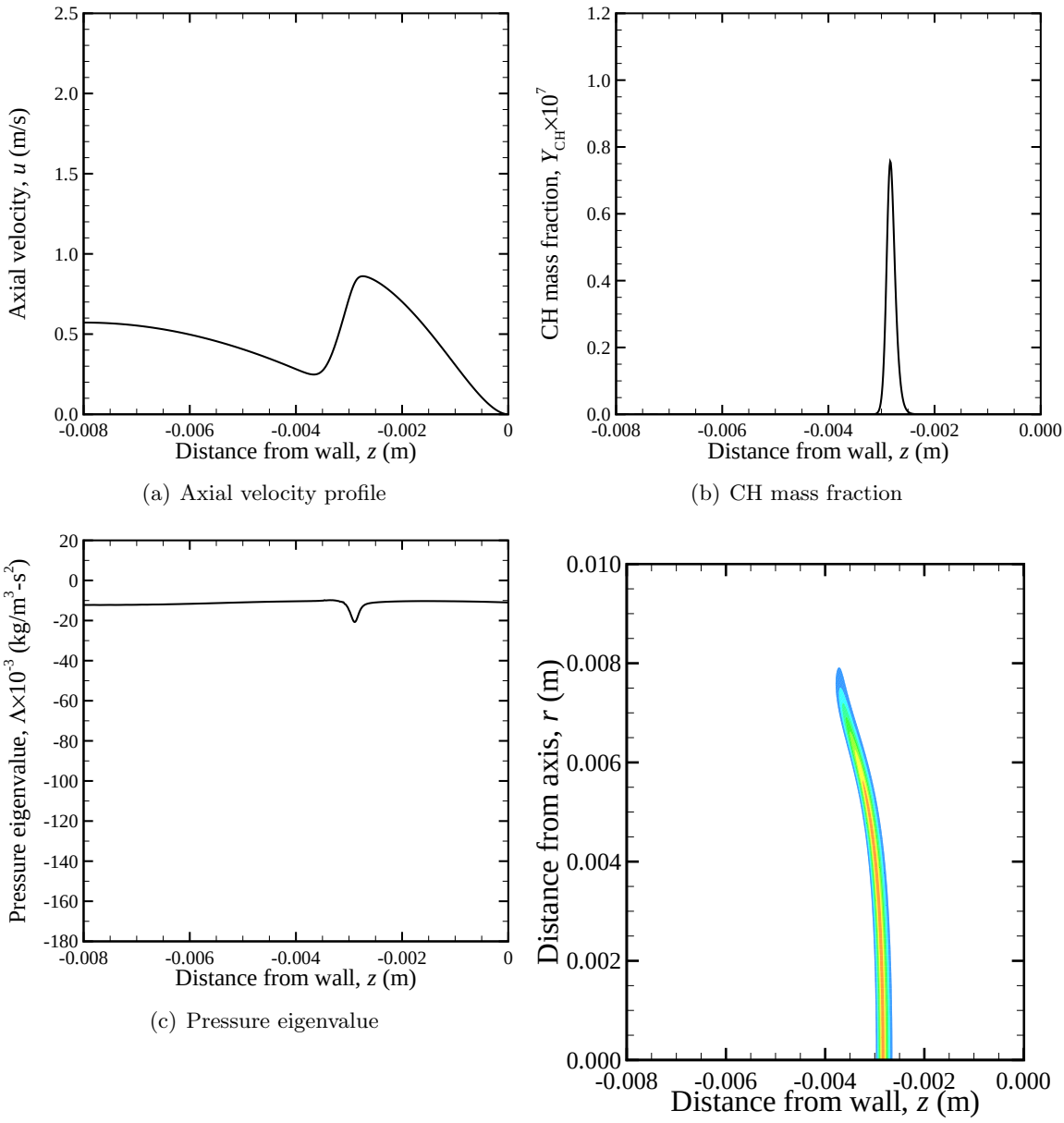

(a) Axial velocity profile

(b) CH mass fraction

(c) Pressure eigenvalue

(d) CH contour

Figure C.6: Φ=0.70, Case B070-27

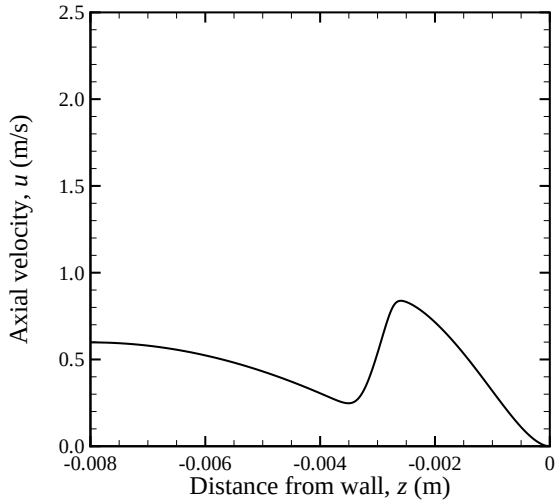

(a) Axial velocity profile

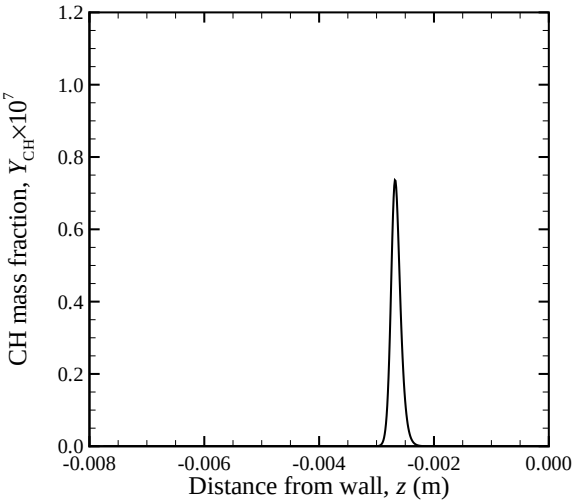

(b) CH mass fraction

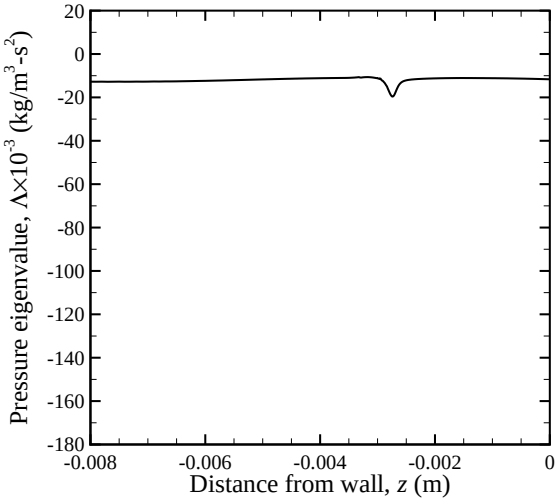

(c) Pressure eigenvalue

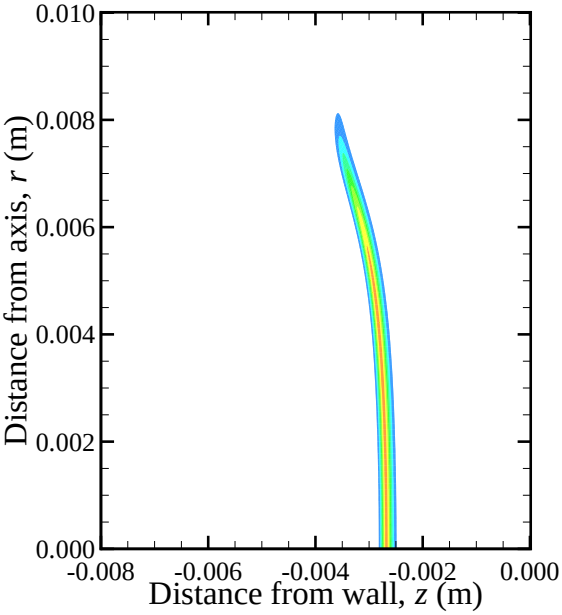

(d) CH contour

Figure C.7: Φ=0.70, Case B070-30

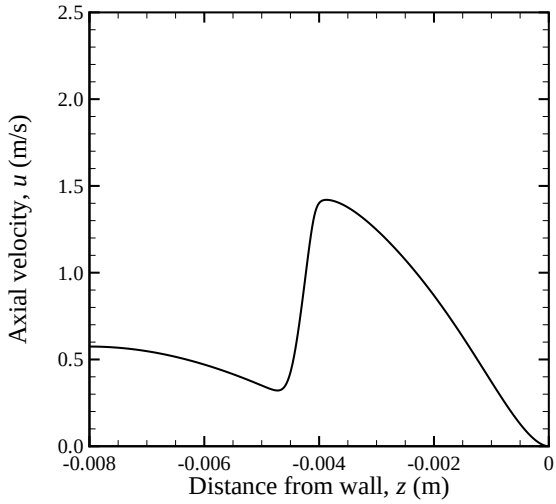

(a) Axial velocity profile

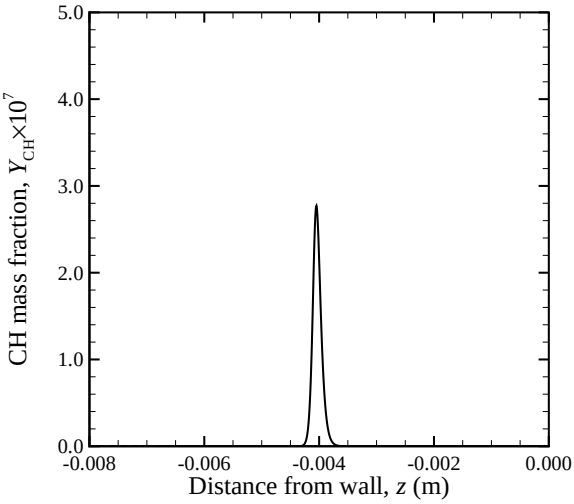

(b) CH mass fraction

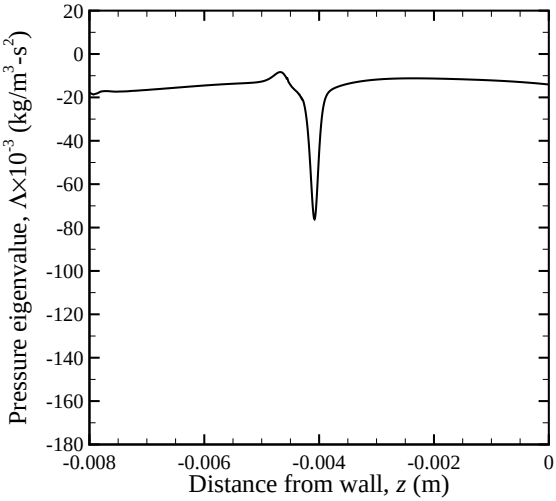

(c) Pressure eigenvalue

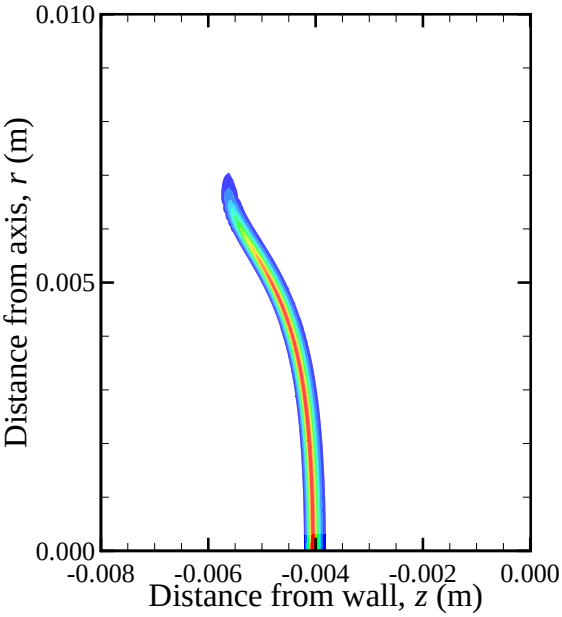

(d) CH contour

Figure C.8: Φ=0.80, Case B080-17

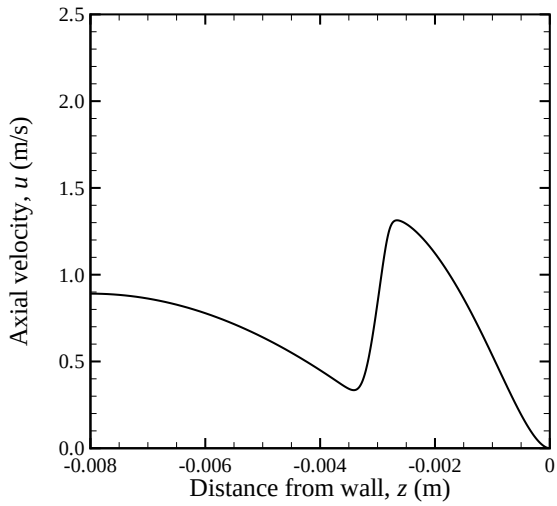

(a) Axial velocity profile

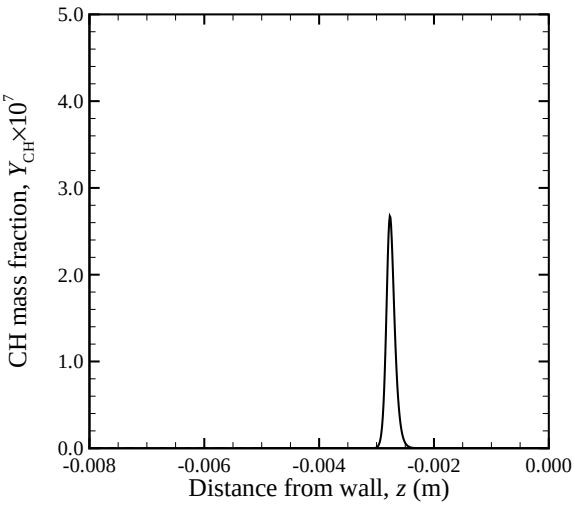

(b) CH mass fraction

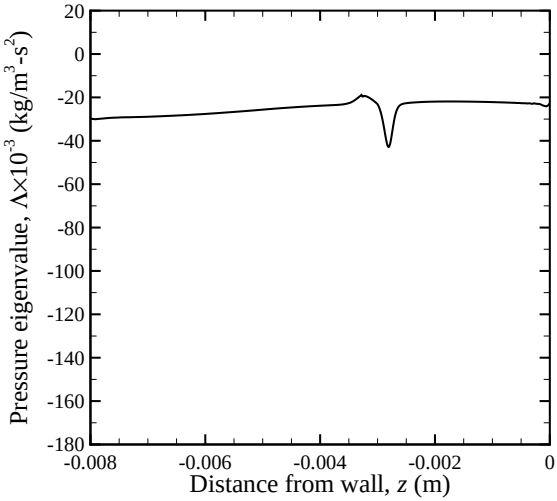

(c) Pressure eigenvalue

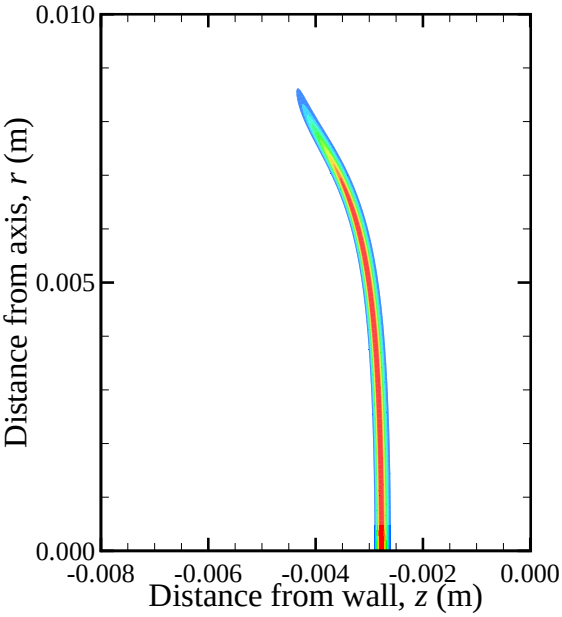

(d) CH contour

Figure C.9: Φ=0.80, Case B080-46

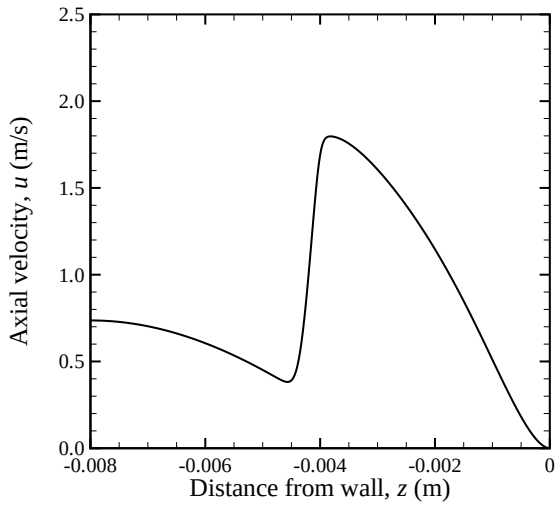

(a) Axial velocity profile

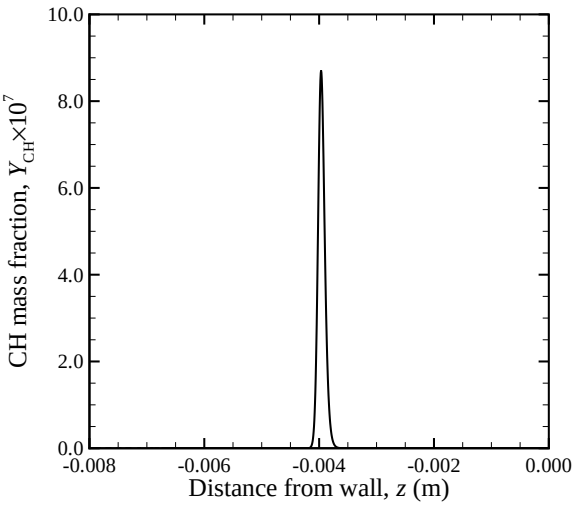

(b) CH mass fraction

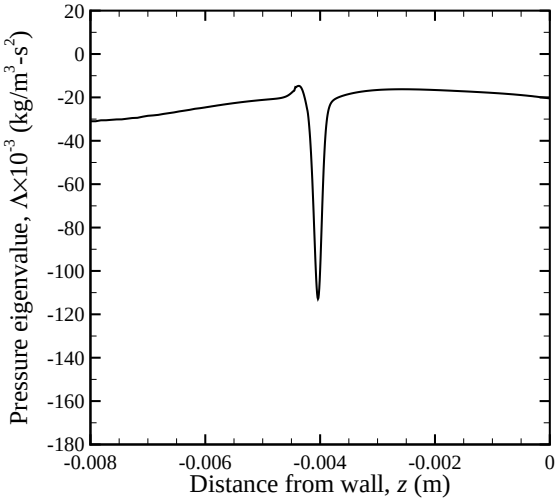

(c) Pressure eigenvalue

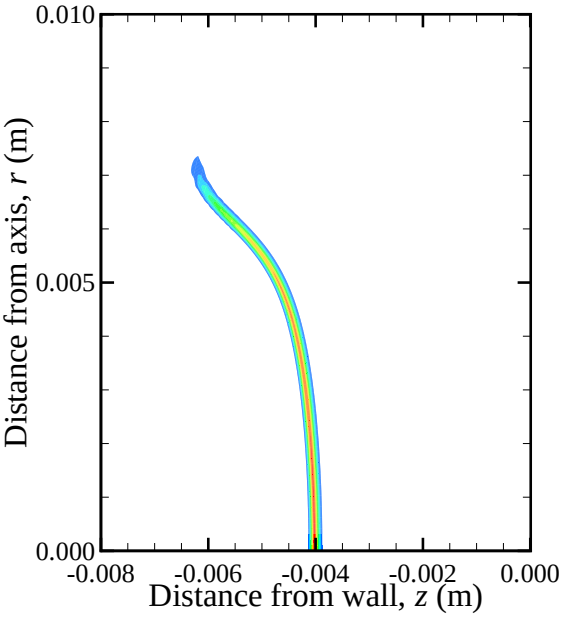

(d) CH contour

Figure C.10: Φ=0.90, Case B090-30

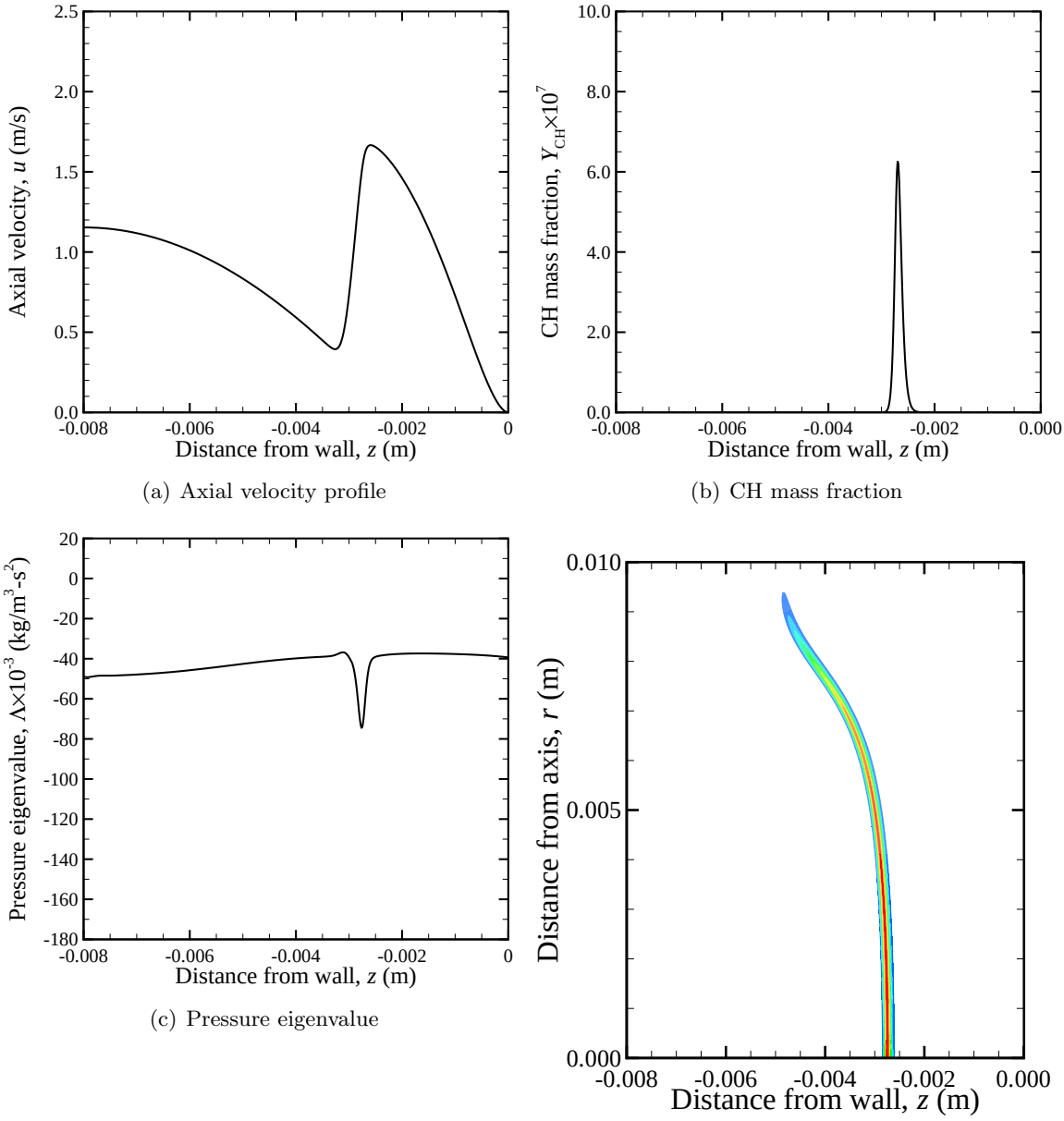

(a) Axial velocity profile

(b) CH mass fraction

(c) Pressure eigenvalue

(d) CH contour

Figure C.11: Φ=0.90, Case B090-50

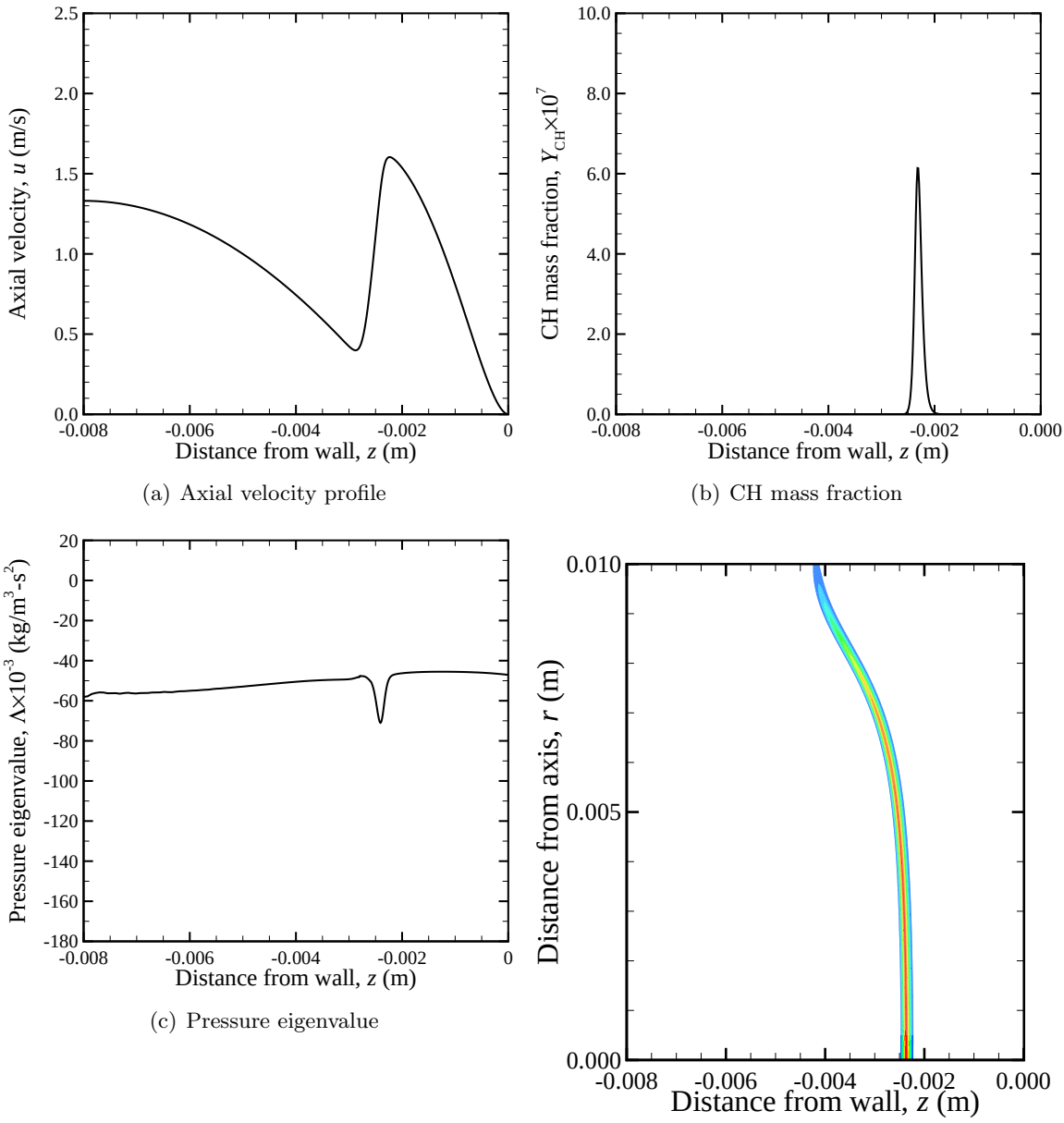

(a) Axial velocity profile

(b) CH mass fraction

(c) Pressure eigenvalue

(d) CH contour

Figure C.12: Φ=0.90, Case B090-106

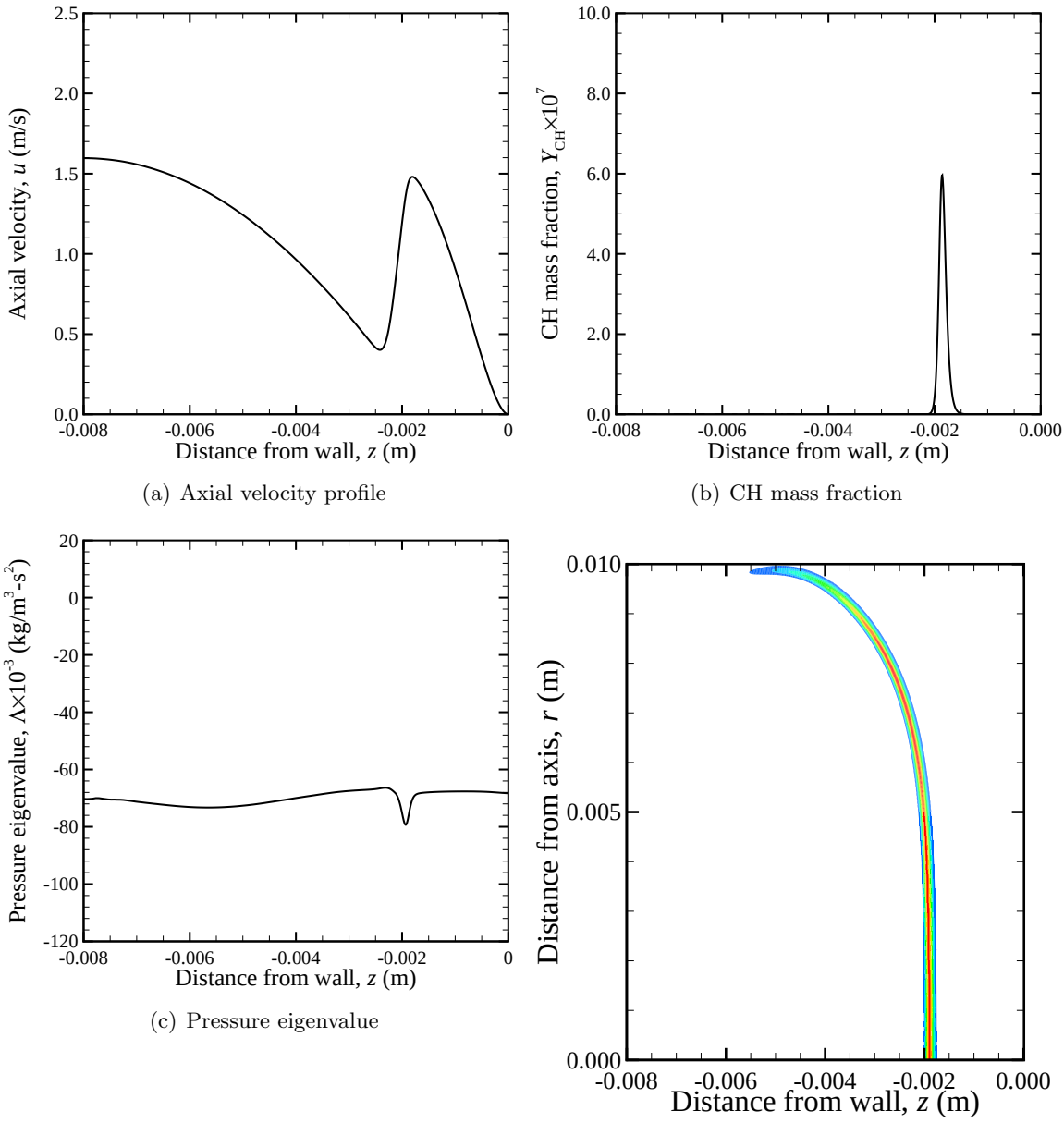

(a) Axial velocity profile

(b) CH mass fraction

(c) Pressure eigenvalue

(d) CH contour

Figure C.13: Φ=0.90, Case B090-112

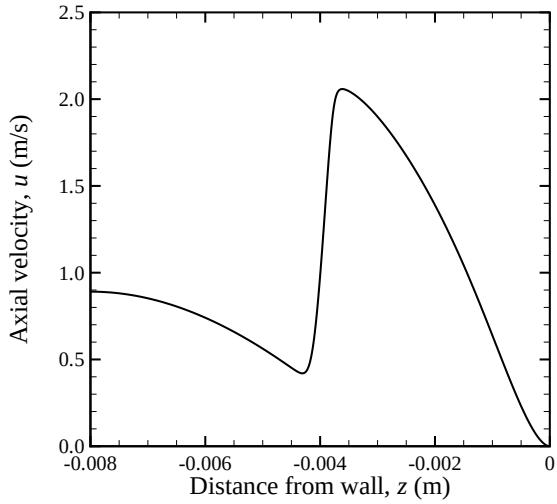

(a) Axial velocity profile

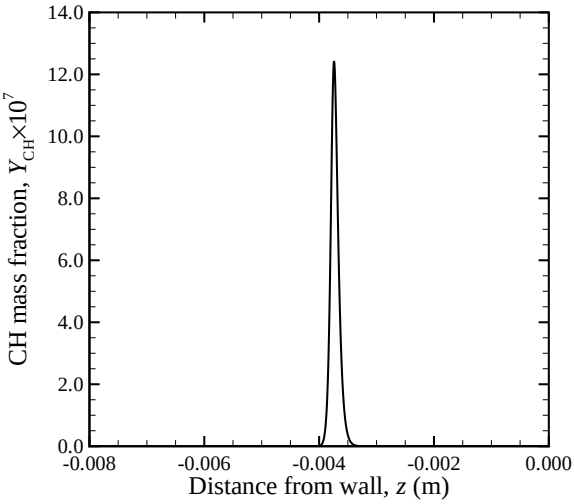

(b) CH mass fraction

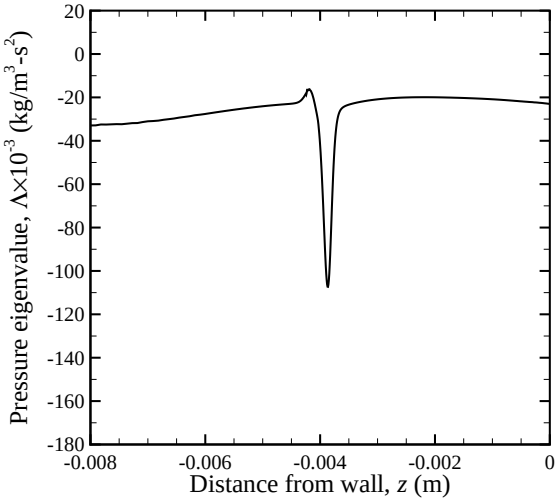

(c) Pressure eigenvalue

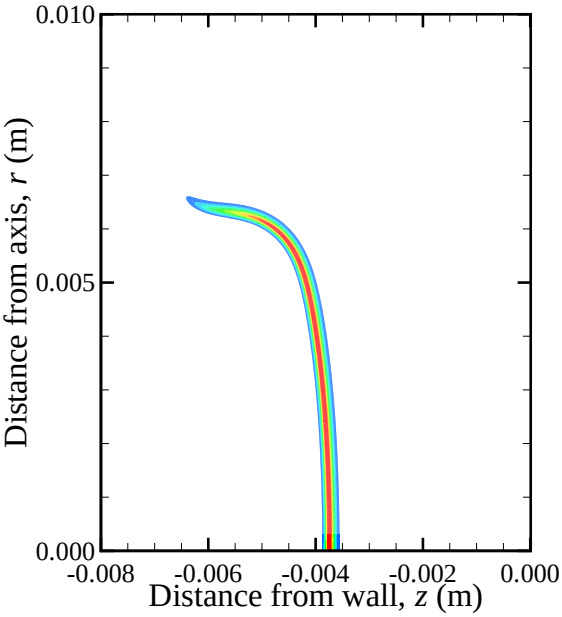

(d) CH contour

Figure C.14: Φ=1.00, Case B100-23

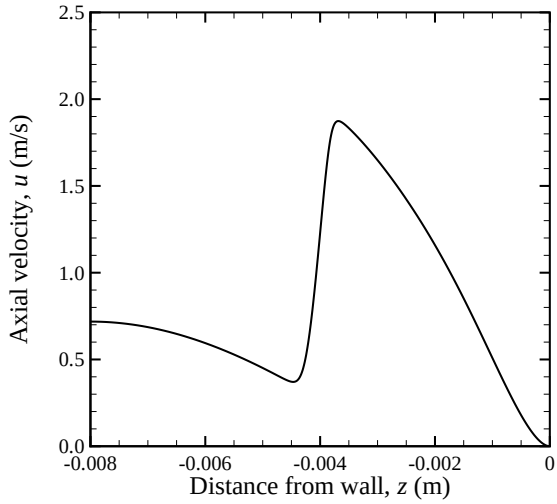

(a) Axial velocity profile

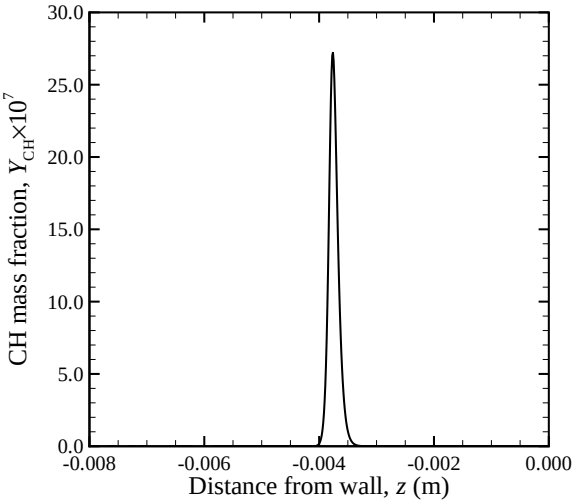

(b) CH mass fraction

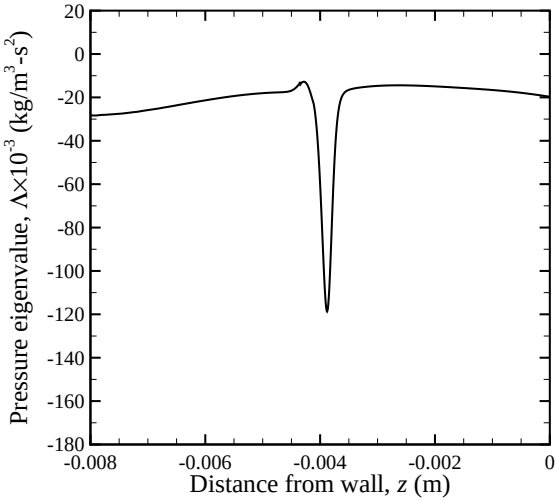

(c) Pressure eigenvalue

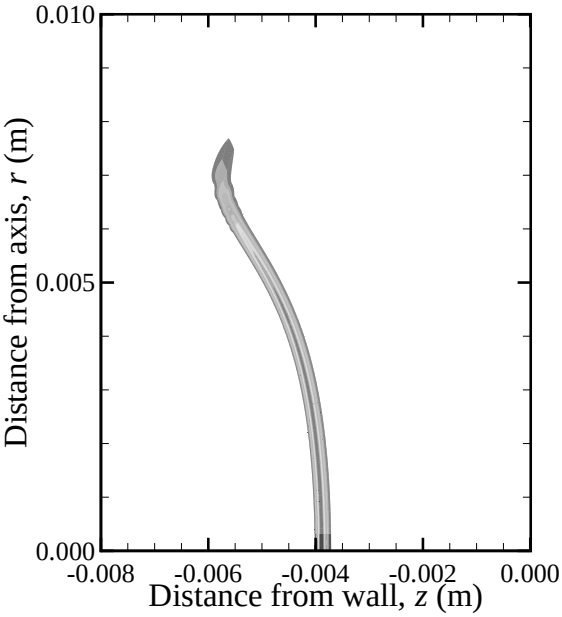

(d) CH contour

Figure C.15: Φ=1.20, Case B120-10

C.2 Phase III: 2D simulation of laboratory flames

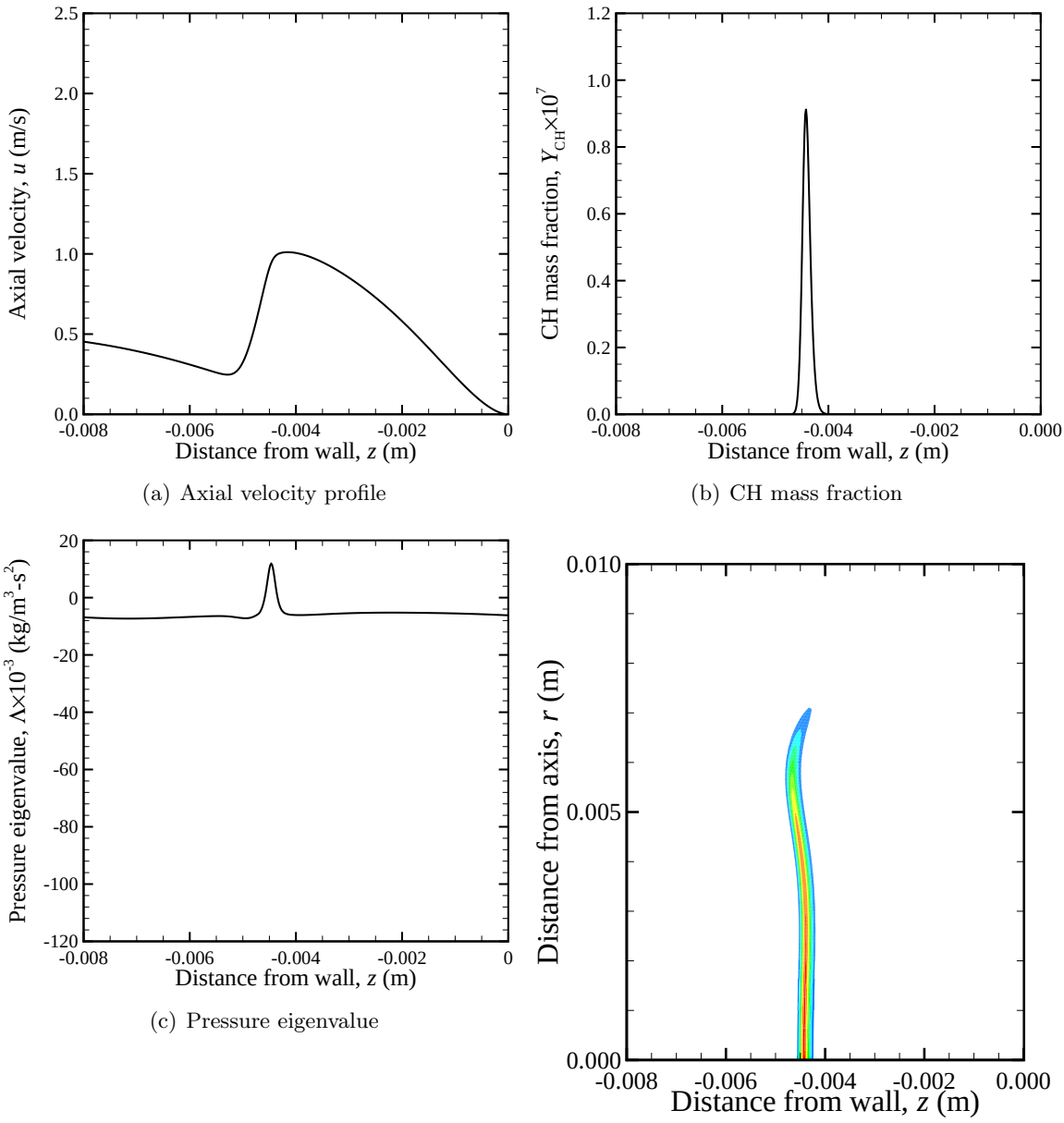

(a) Axial velocity profile

(b) CH mass fraction

(c) Pressure eigenvalue

(d) CH contour

Figure C.16: Φ=0.70, Case C070-4

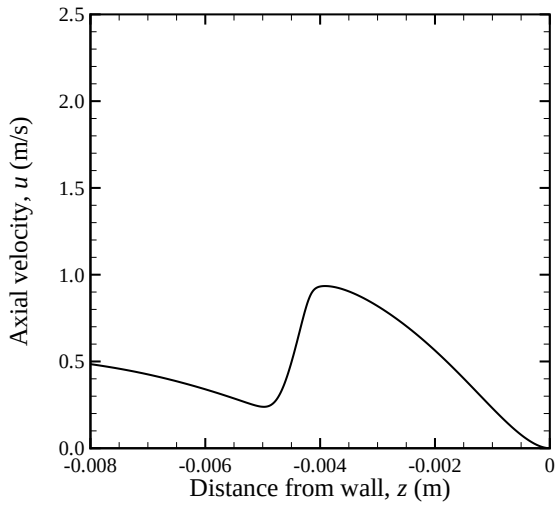

(a) Axial velocity profile

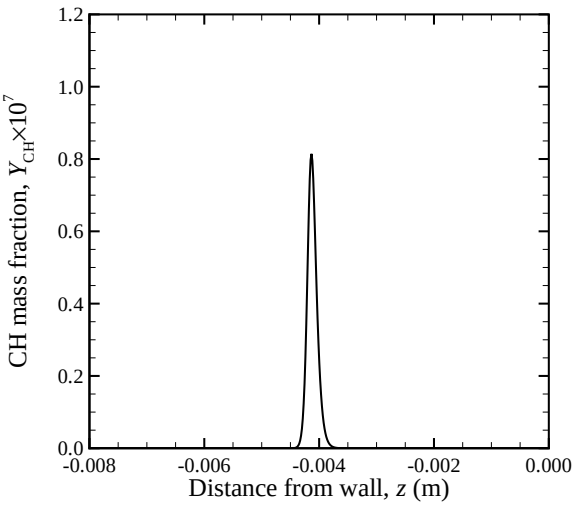

(b) CH mass fraction

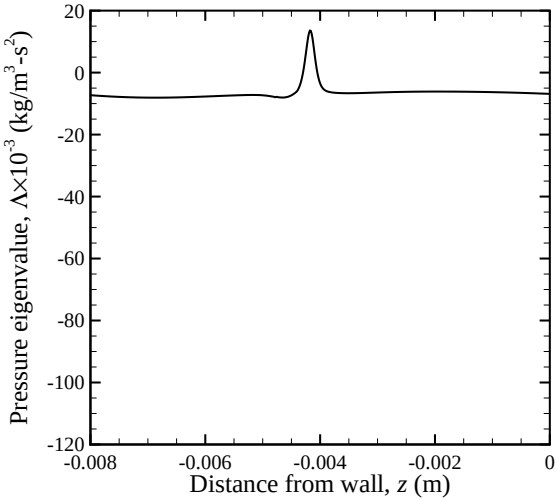

(c) Pressure eigenvalue

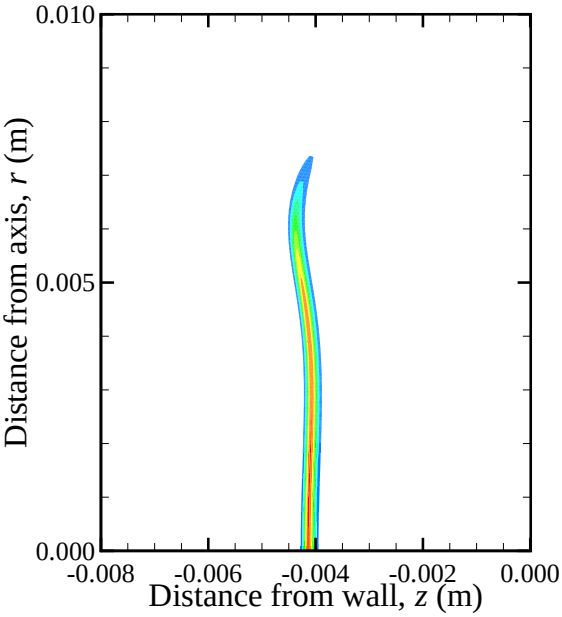

(d) CH contour

Figure C.17: Φ=0.70, Case C070-11

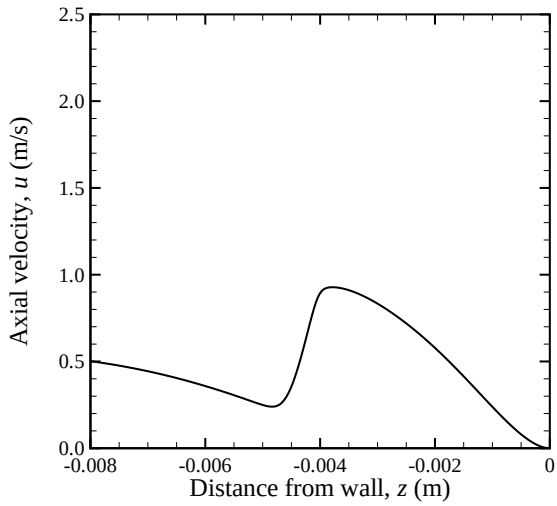

(a) Axial velocity profile

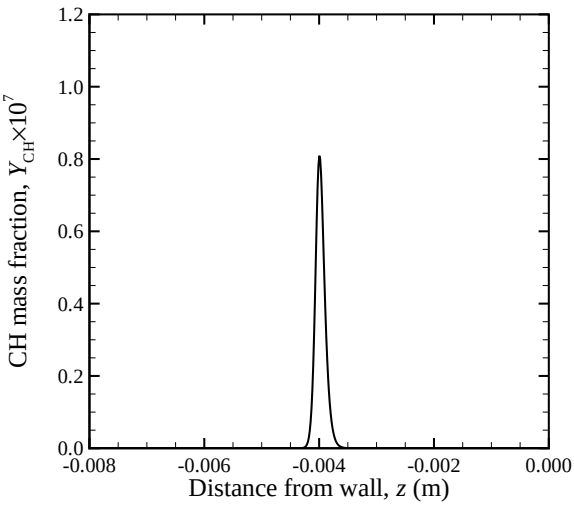

(b) CH mass fraction

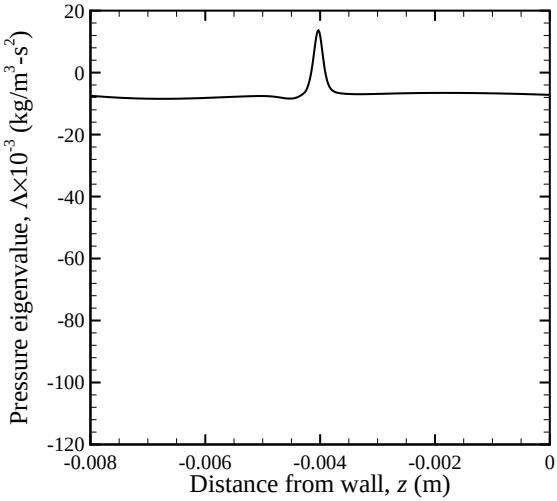

(c) Pressure eigenvalue

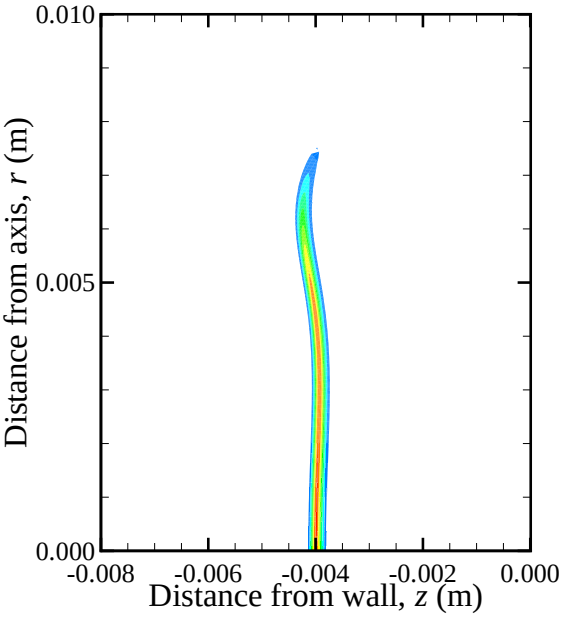

(d) CH contour

Figure C.18: Φ=0.70, Case C070-8

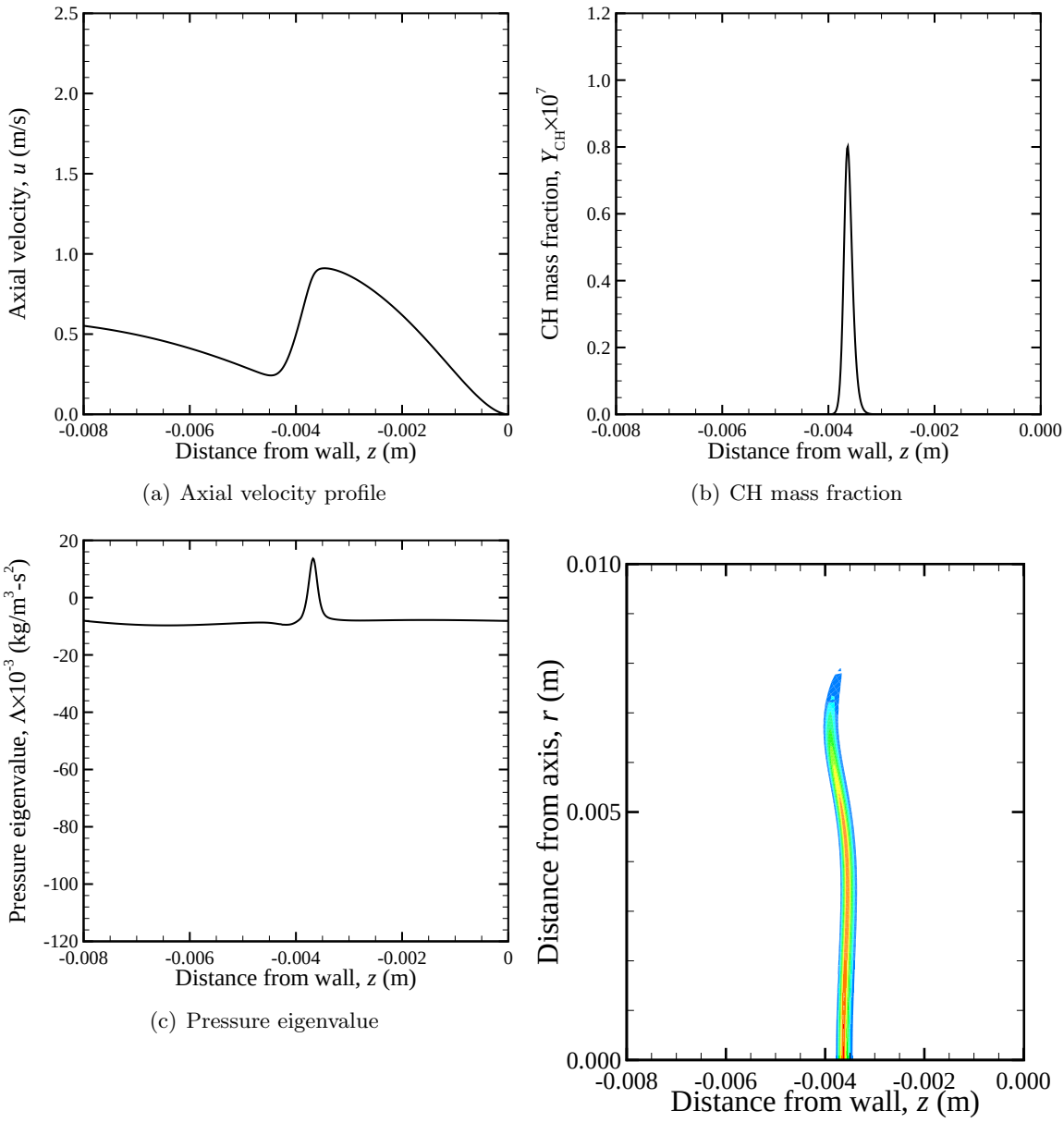

(a) Axial velocity profile

(b) CH mass fraction

(c) Pressure eigenvalue

(d) CH contour

Figure C.19: Φ=0.70, Case C070-9

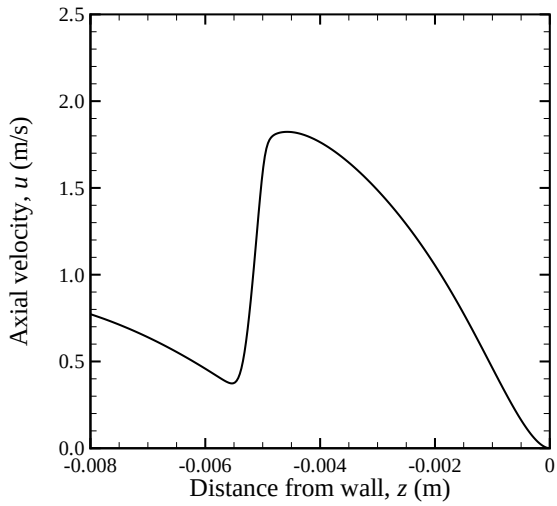

(a) Axial velocity profile

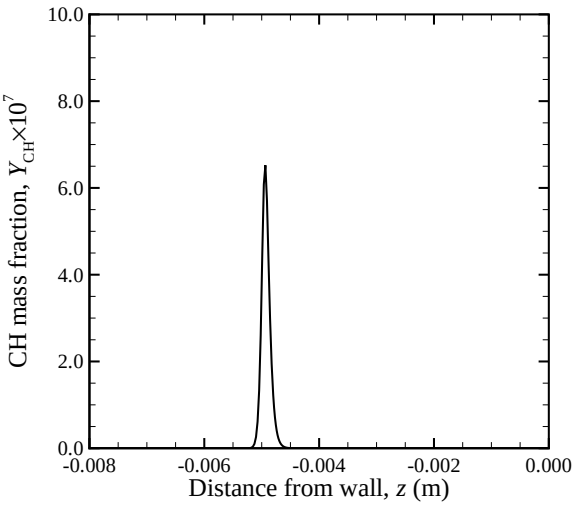

(b) CH mass fraction

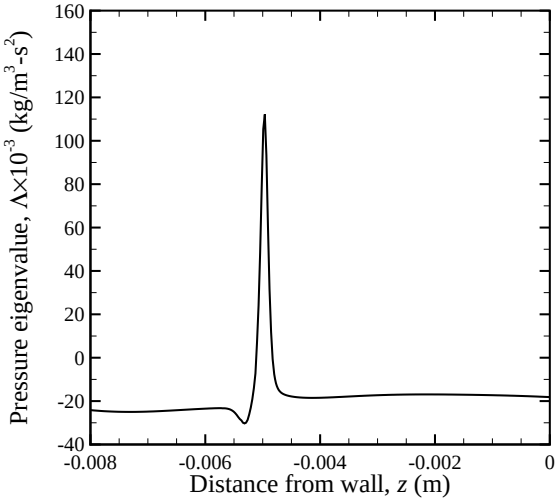

(c) Pressure eigenvalue

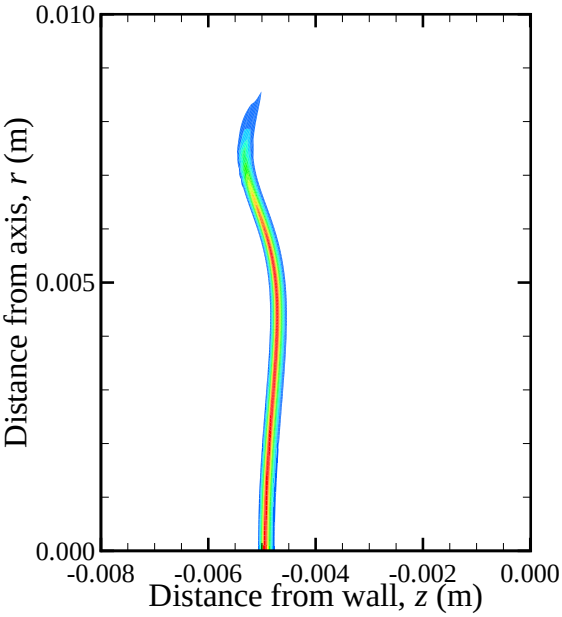

(d) CH contour

Figure C.20: Φ=0.90, Case C090-5

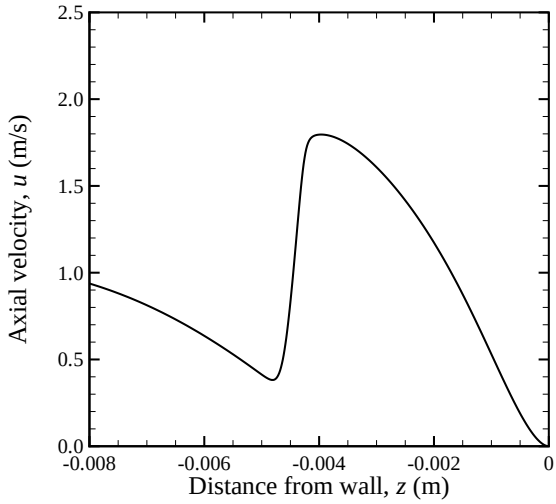

(a) Axial velocity profile

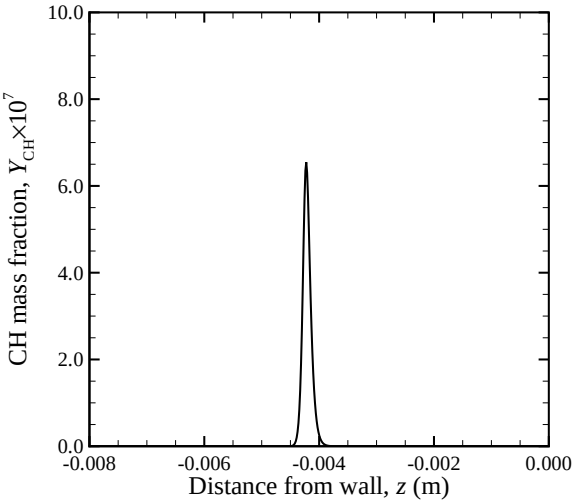

(b) CH mass fraction

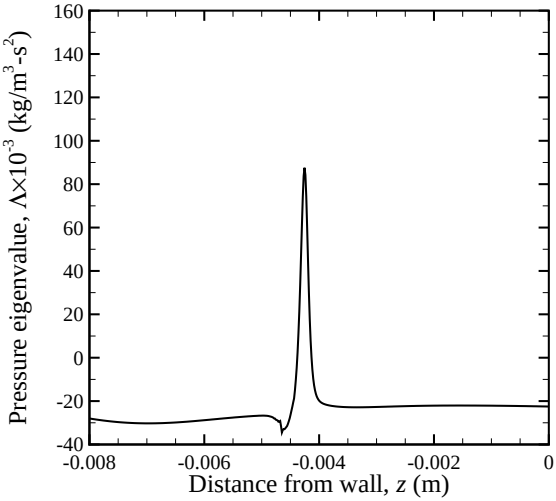

(c) Pressure eigenvalue

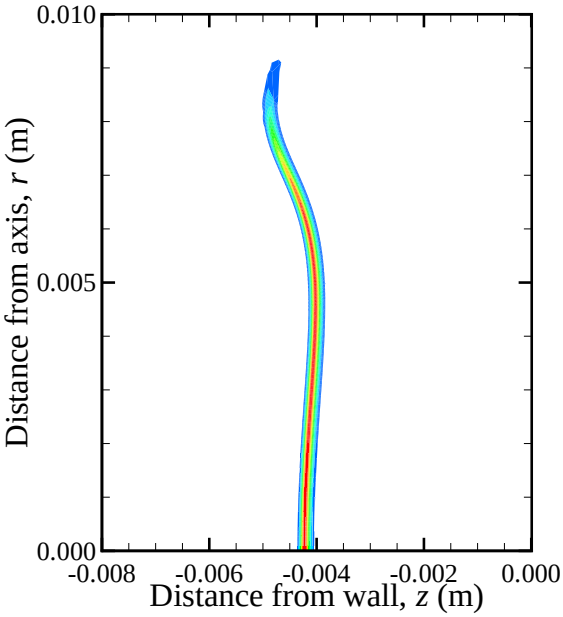

(d) CH contour

Figure C.21: Φ=0.90, Case C090-2

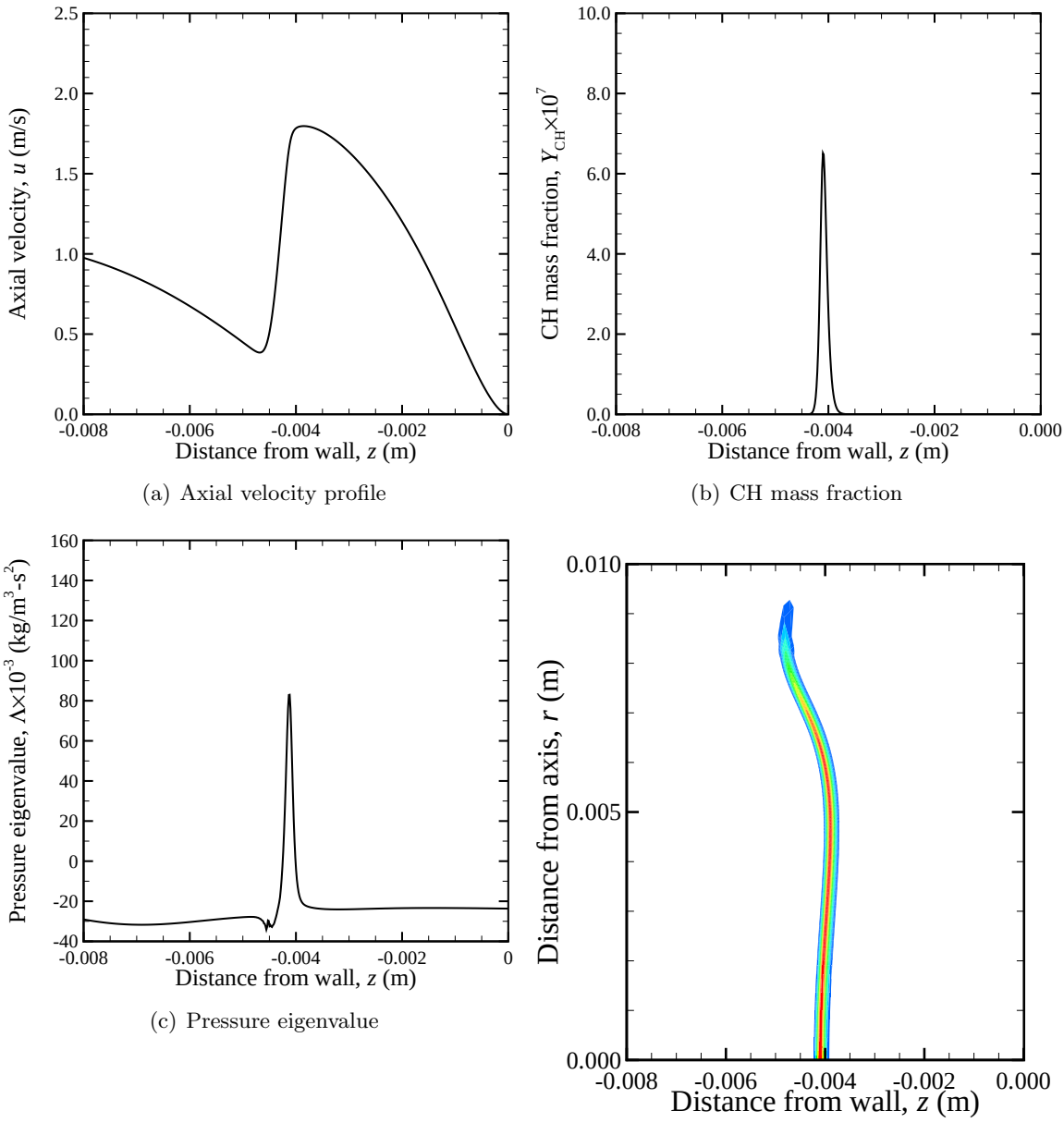

(a) Axial velocity profile

(b) CH mass fraction

(c) Pressure eigenvalue

(d) CH contour

Figure C.22: Φ=0.90, Case C090-4

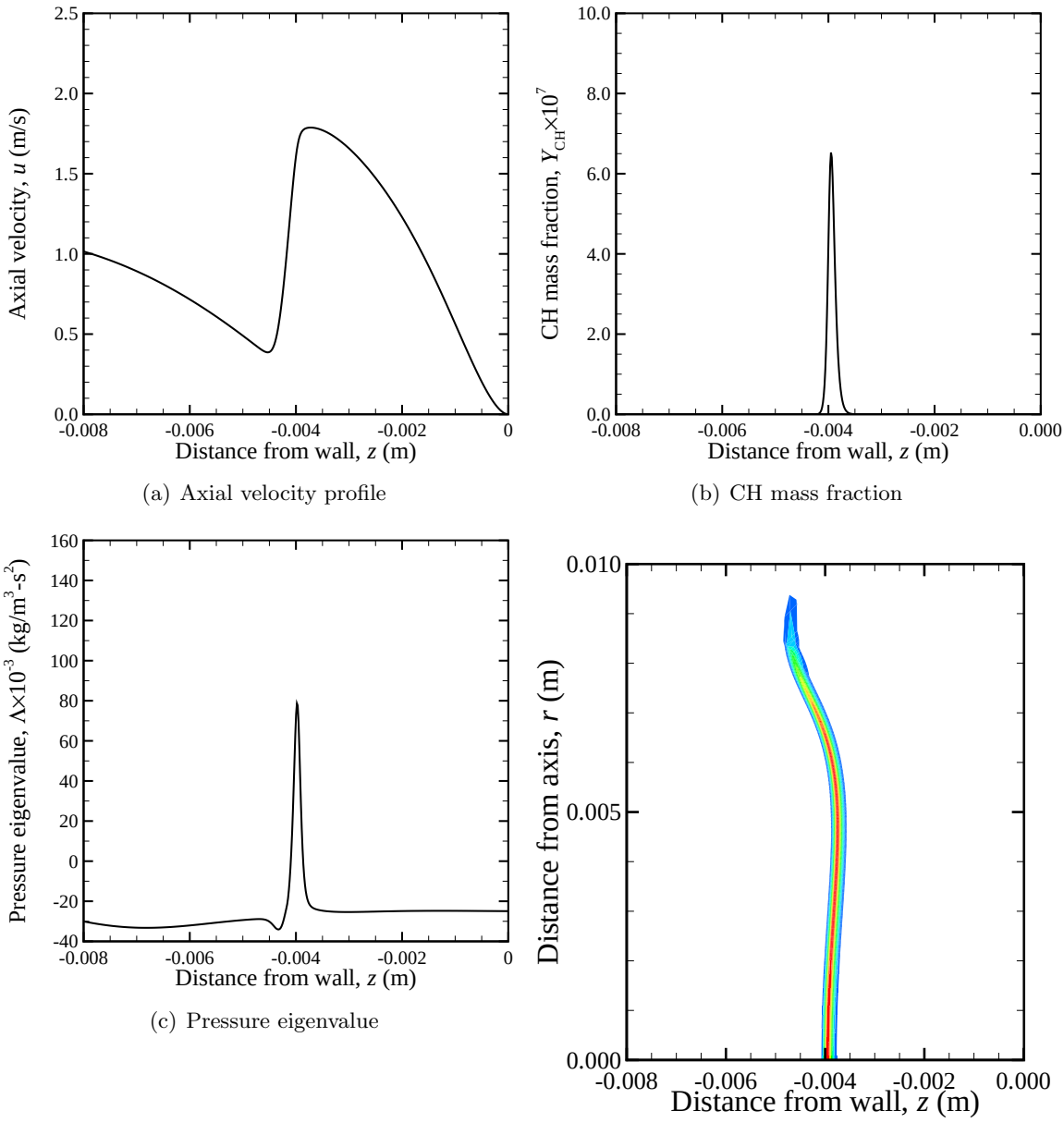

(a) Axial velocity profile

(b) CH mass fraction

(c) Pressure eigenvalue

(d) CH contour

Figure C.23: Φ=0.90, Case C090-3

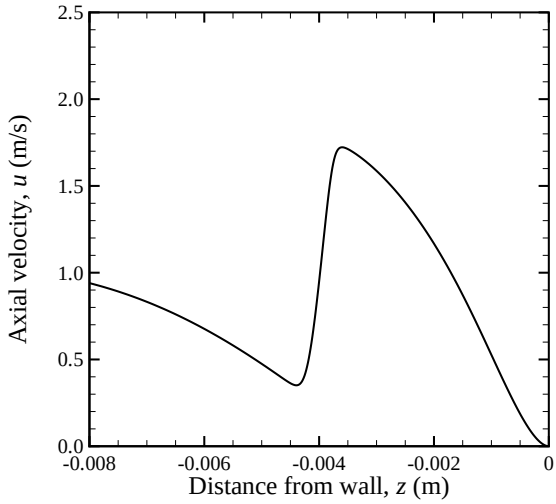

(a) Axial velocity profile

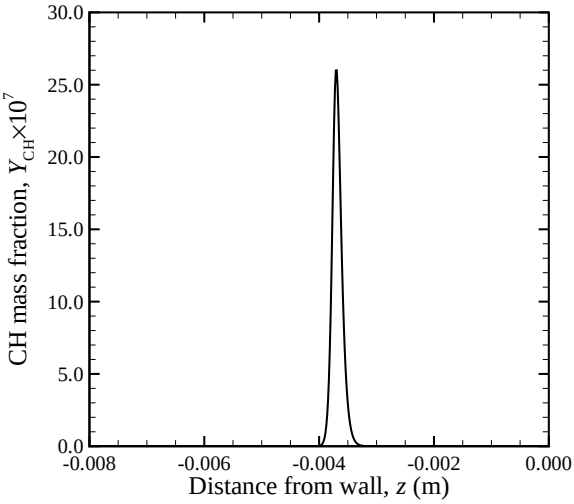

(b) CH mass fraction

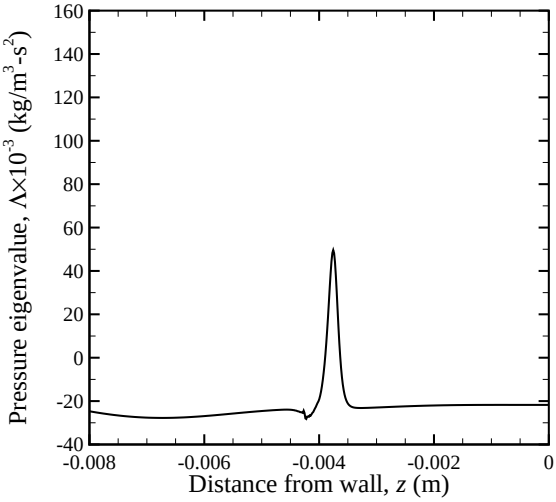

(c) Pressure eigenvalue

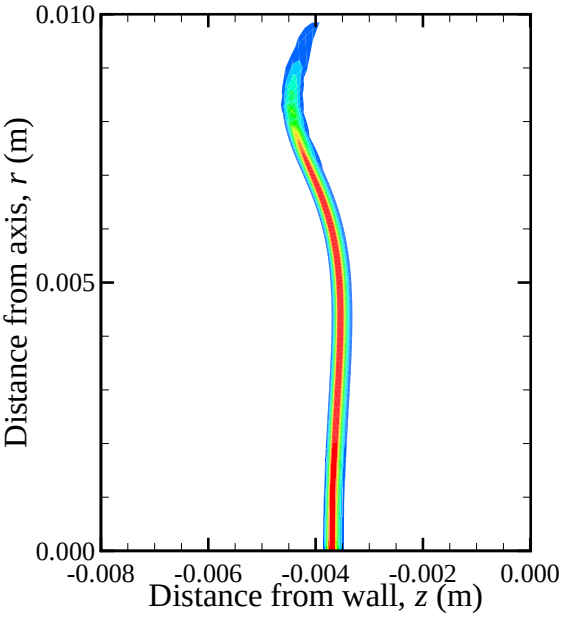

(d) CH contour

Figure C.24: Φ=1.20, Case C120-1

Appendix D

Post-simulation analysis tool

D.1 PSV velocity simulation

The following *MATLAB*®script takes one-dimensional flow data and computes a particle motion. By filtering the particle motion as done in the laboratory, a simulation of PSV-measured velocity data can be obtained. For more details, Bergthorson (2005) should be consulted. The script was originally written by Jeff Bergthorson, with improvements made by the author and Laurent Benezech. It is included here for an archival purpose.

```
% PSV: PSV velocity correction.
% This program computes what PSV velocity data should be given simulation
% velocity data.
%
% USAGE: [PM, PSV, PFORCE, converged] = psv(data)
% returns the particle motion (PM) data and particle-streak velocimetry
% (PSV) data as well as three forces acting on a particle at each point.
% PM contains three columns.  The first column is the position of the
% particle.  The second is the velocity of the particle at that point and
% the third column is the acceleration of the particle at that point.  PSV
% contains two columns.  The first column is the position where the
% computed PSV velocity is defiend and the second column is the
% corresponding velocity data.  PFORCE contains three columns: Stokes drag,
% Thermophoretic force and gravity.  Each row corresponds to the first
% column of PM where particle locations are specified.  converged is a
```

```
% single integer value that returns 1 if the integration was successful and
% the particle reached to the end of the domain and 0 otherwise.  The
% function takes one to five input arguments.  The first input is the
% simulation data, which is mandatory and must be arranged in the following
% order: [x u V T r M mu] where the first column (x) is the axial position,
% u is the axial velocity, V is the spreading rate, dv/dr, T is the
% temperature, r is the density, M is the average molecular weight and mu
% is the mixture gas viscosity. It is assumed the data is stored such that
% it is an increasing order in x.  The second to sixth inputs are optional.
% The second input argument can by 'Al2O3', 'Zeeo' or user-specified
% particle properties.  When particle properties are specified, it must be
% 1x3 cell with the first cell being the particle diameter (m), the second
% being the particle density (Kg/m^3) and the last one is the thermal
% conductivity of the particle.  This can be a single number (constant
% thermal conductivity), or an array with the first column being
% temperature and the second column being the corresponding thermal
% conductivity at the given temperature.  (See example below)  When
% particle data is omitted, 'Zeeo' is used by default.  The third to sixth
% parameters are, the chopping frequency of the PSV, max iteration of
% temporal integration of particle motion, the number of subiterations
% within each PSV chopping cycle and the integration order (1 or 2).  When
% omitted, 1600, 100000, 100 and 2 are used by default respectively.
%
% example 1:
% psv(simdata, {1.0e-5, 1000, 1.0}): simulates a particle whose diameter is
% 10 microns, density is 1000 (kg/m^3), and the thermal conductivity is 1
% (W/m-K) at all temperature.
%
% example 2:
% psv(simdata, {3.0e-6, 2400, [300 100.0; 2000 1000.0]}: simulates a
% particle whose diameter is 3 microns, density is 2400 (kg/m^3), and the
% thermal conductivity is 100 (W/m-K) at 300K and 1000 (W/m-K) at 2000 K.
```

```
% At other temperature, the conductivity is linearly interpolated or
% extrapolated.
%
% example 3:
% psv(simdata, 'Al2O3', 2400, 250000, 200) : simulates a motion of Al2O3
% particle with PSV chopping frequency of 2400.  It tries to iterate up to
% a quater of million iterations at a time step of 1/2400 x 1/200.
%
% For more details, Jeff Bergthorson's thesis should be consulted.
%
% AUTHORS: Jeff M. Bergthorson, Laurent Benezech, and Kazuo Sone.
%
function [PM, PSV, PFORCE, converged] = psv(flowData, varargin)

narg = size(varargin,2);

if (nargin < 1)
   error('psv:NumInputs','Not enough input arguments.');
end

%%% Parameter definitions. %%%
if narg < 1
    % When particle is not specified, use 'Zeeo' as default.
    param = 'Zeeo';
else
    param = varargin{1};
end

% Particle properties, {diameter, density, conductivity}.

if iscell( param )
    % This is the case when property is specified by user.
```

```
    % dpart: Diameter of the particle.
    dpart = param{1};
    % rhopart: Particle density in kg/m^3
    rhopart = param{2};
    pcond = param{3};
else
    % Use preset values.
    if strcmp( param, 'Al2O3' )
        dpart = 1.0e-6;     % (m)
        rhopart = 3830.0;   % (Kg/m^3)
        %Thermal conductivity of particles Incropera and deWitt
        % - Fundamentals of Heat and Mass Transfer, 3rd edition 1990
        pcond = [200 55;
            400 26.4;
            600 15.8;
            800 10.4;
            1000 7.85;
            1200 6.55;
            1500 5.66;
            2000 6;
            2500 6.4];
    elseif strcmp( param, 'Zeeo' )
        dpart = 3.0e-6;     % (m)
        rhopart = 2400.0;   %(kg/m^3)
        pcond = 2.3;        % (W/mK)
    else
        % Error!
        error('psv:ParticleInfo','Particle specification incorrect.');
    end
end

% frequency: Chopping frequency of PSV.
```

```
if narg > 1
    frequency = varargin{2};
else
    frequency = 1600;
end

% max_iterations: Maximum number of integration steps.
if narg > 2
    max_iterations = varargin{3};
else
    max_iterations=100000;
end

% nsubcycle: number of iterations to get 1 PSV cycle.
% Default value is 100.
if narg > 3
    nsubcycle = uint16( varargin{4} );
else
    nsubcycle = 100;
end

% integorder: Order of time integration (1 or 2).
% Default value is 2.
% Use 1st order only when speed is important.
if narg > 4
    integorder = uint16( varargin{5} );
    if integorder < 1 || integorder > 2
        error('psv:IntegOrder', ...
              'Incorrect integration order.  Must be 1 or 2');
    end
else
    integorder = 2;
```

```
end

% deltat: Integration of particle equations.
deltat = 1/frequency * 1/double(nsubcycle);
% halfdeltat: 1/2 deltat (used in 2nd order method)
halfdeltat = 0.5 * deltat;

%%% Universal constants. %%%
% Using the simulated flow, temperature and property fields,
% we need to model a particles behavior as it traverses the flowfield.
%Gravitational acceleration
a_gravity=9.81; %m/s^2

% mpart: Mass of the particle
mpart=rhopart*pi*4/3*(dpart/2)^3; %in kg;
%
% End of parameters.
%

xsim=flowData(:,1);
lsim=max(xsim); % End of the simulation domain.

usim=flowData(:,2);
Vsim=flowData(:,3);
T=flowData(:,4);
rho=flowData(:,5);
Mbar=flowData(:,6);
visc=flowData(:,7);

gradT=zeros(size(flowData,1),1);
for i=2:1:size(flowData,1)-1;
    gradT(i)=(T(i+1)-T(i-1))/(xsim(i+1)-xsim(i-1));
```

```
end
gradT(size(flowData,1))=gradT(size(flowData,1)-1);

%
%Initialize the particle with a corrected particle velocity and
%acceleration
i = 1;
tpart(1)=0;
xpart(1)=0;

% CKWp: approximately 1+1.142*Kn for small Kn.
%     : see Eqn.(A.10) in Jeff Bergthorson's thesis.
CKWp(1)=1.05;

% vpart: Eqns.(A.23) & (A.24) in Jeff Bergthorson's thesis
%      : vpart/vfluid = 1/(1+C_KW*tau_S*sigma_f)
%      : sigma_f = du/dx.
dudx = -2*Vsim(1);
vpart(1)=usim(1)/(1+CKWp(1)*(rhopart*dpart^2/(18*visc(1)))*dudx);
% ufp: fluid velocity at particle location.
ufp(1)=usim(1);
[apart(1), F_thermophoretic(1), F_stokes(1)] = ...
    Particle_acceleration(mpart, dpart, pcond, vpart(1), ...
                          [ufp(1) T(1) gradT(1) rho(1) Mbar(1) visc(1)]);

%The gravitational force is a constant and can be calculated prior to the
%loop
F_gravity=-mpart*a_gravity;

continue_iteration = 1;
while continue_iteration
    % Increment time by deltat, and update x, u,and a through 1st order
```

```
% explicit Euler method of integration.
i = i + 1;
tpart(i)=tpart(i-1)+deltat;
xpart(i)=xpart(i-1)+deltat*vpart(i-1);
vpart(i)=vpart(i-1)+deltat*apart(i-1);

% Interpolate the simulated fields at the particle location.
flow_at_particle = interp1(xsim, [usim T gradT rho Mbar visc], ...
                           xpart(i), [], 'extrap');

if integorder == 2
    apart(i) = Particle_acceleration(mpart, dpart, pcond, vpart(i), ...
                                     flow_at_particle);

    % Apply second order correction (2nd order Runge-Kutta method)
    xpart(i) = xpart(i-1) + halfdeltat*(vpart(i-1)+vpart(i));
    vpart(i) = vpart(i-1) + halfdeltat*(apart(i-1)+apart(i));

    % Interpolate the simulated fields at the particle location.
    flow_at_particle = interp1(xsim, [usim T gradT rho Mbar visc], ...
                               xpart(i), [], 'extrap');
end

[apart(i), F_thermophoretic(i), F_stokes(i)] = ...
    Particle_acceleration(mpart, dpart, pcond, vpart(i), ...
                          flow_at_particle);

% Check if the particle has reached to the wall close enough.
% and if so, exit the loop.
% Note xpart has been computed way above here, but I have to get apart
% otherwise the resulting array does not have the same number of rows.
if xpart(i) >= lsim || i > max_iterations
```

```
        continue_iteration = 0;
    end
end

% Issue an warning message if not converged.
if i > max_iterations
    converged = 0;
    warning('Iteration may not have converged.  ');
    warning('Increase maximum number of iterations.');
else
    converged = 1;
end

%now want to estimate the PSV velocity from this flowfield.
nb0 = nsubcycle+1;
nb1 = size(tpart,2);
ne0 = 1;
ne1 = size(tpart,2)-nsubcycle;
PSV(:,1) = (xpart(nb0:nb1)+xpart(ne0:ne1)) * 0.5;
PSV(:,2) = (xpart(nb0:nb1)-xpart(ne0:ne1)) * frequency;

% Assign to the returning matrix.
PM = [xpart; vpart; apart]';
PFORCE = [F_stokes; F_thermophoretic; F_gravity*ones(1,i)]';

%-------------------------
% Private functions
%-------------------------

%--------------------------------------------------------------------------
% Particle_acceleration: This function computes a particle acceleration.
function [apart, F_thermophoretic, F_stokes] = ...
```

```
    Particle_acceleration(mpart, dpart, pcond, vpart, flow_p)

ufp = flow_p(1);
Tp = flow_p(2);
gradTp = flow_p(3);
rhop = flow_p(4);
Mbarp = flow_p(5);
viscp = flow_p(6);

% R_univ: Universal gas constant.
R_univ=8314; %J/kmolK

% kftransp: The tranlational part of the thermal conductivity
%         : See Eqn.(A.26) in Jeff's thesis.
kftransp = 15*R_univ*viscp/(4*Mbarp);

% kpp : Thermal conductivity of the particle.  When it is not a function of
% temperature, use it.  If it is a function of temperature, pcond should be
% given by a table - simply interpolate.
if length(pcond) == 1
    kpp = pcond;
else
    kpp = interp1(pcond(:,1), pcond(:,2), Tp, [], 'extrap');
end

% Now calculate the parameters needed for the forces:
% Knp: Knudsen number.
Knp = Knudsen_number(Tp, Mbarp, viscp, rhop, dpart, R_univ);

% CKWp: Eqn.(A.10)
CKWp = 1+Knp*[1.142+0.558*exp(-0.999/Knp)];
```

```
%Now calculate the thermophoretic and stokes drag forces:
F_thermophoretic = Force_Thermophoretic_Talbot(viscp, dpart, rhop, ...
                                                kftransp, kpp, Knp, gradTp, Tp);
F_stokes = Force_Stokes(viscp, dpart, vpart, ufp, CKWp);

%Calculate the acceleration: Eqn.(A.7)
apart = (F_stokes+F_thermophoretic)/mpart;
%--------------------------------------------------------------------------

%--------------------------------------------------------------------------
% Force_Stokes: This function computes stokes drag.
function [F_stokes] = Force_Stokes(viscp, dpart, vpart, ufp, CKWp)

%Stokes drag: Eqn.(A.9)
F_stokes = -3*pi*viscp*dpart*(vpart-ufp)/CKWp;
%--------------------------------------------------------------------------

%--------------------------------------------------------------------------
% Force_Thermophoretic_Talbot: This function computes thermophoretic force
% by Talbot's model.
function [F_tp] = Force_Thermophoretic_Talbot(viscp, dpart, rhop, ...
                                                kftransp, kpp, Knp,gradTp, Tp)

%Talbot: Eqn.(A.28)
num = -(6*pi*viscp^2/rhop*dpart*1.17*(kftransp/kpp+2.18*Knp)*gradTp/Tp);
den = (1+3*1.14*Knp)*(1+2*kftransp/kpp+2*2.18*Knp);
F_tp = num/den;
%--------------------------------------------------------------------------

%--------------------------------------------------------------------------
% Knudsen_number: This function computes Knudsen number
function [Knp] = Knudsen_number(Tp, Mbarp, viscp, rhop, dpart, R_univ)
```

```
% cbarp: Eqn.(A.12)
cbarp = (8*R_univ*Tp/(Mbarp*pi))^0.5;

% Lambdap: Eqn.(A.11)
Lambdap=2*viscp/(rhop*cbarp);

% Knp: Knudsen number.
Knp = 2*Lambdap/dpart;
%-------------------------------------------------------------------------
```

Appendix E

Opposed-jet hydrogen flames and comparison of mechanisms

This appendix is designed to demonstrate the importance of the hydrogen subset of hydrocarbon mechanisms. Understanding hydrogen flame behavior should supplement hydrocarbon combustion models because each hydrocarbon reaction model contains a hydrogen reaction submechanism (see Table 1.1). Figs. E.1–E.4 compare performance of three different hydrogen mechanisms: H1, H2, and H4 in Table 1.1, in the above opposed-jet configuration at the same condition. H2 and H4 tend to show an agreement, in particular, their velocity profile is nearly identical, while the GRI-Mech 3.0 submechanism shows discernible departure from the other two. However, they all disagree in the prediction of hydrogen radical profile. Some of the reactions that appear in the hydrogen reaction submodel have a significant effect on the flame speed of hydrocarbons, as pointed out by several authors (Williams, 2000; Turányi *et al.*, 2002), and refinement in the hydrocarbon kinetics model should come in tandem with understanding of hydrogen reactions, including extinction characteristics.

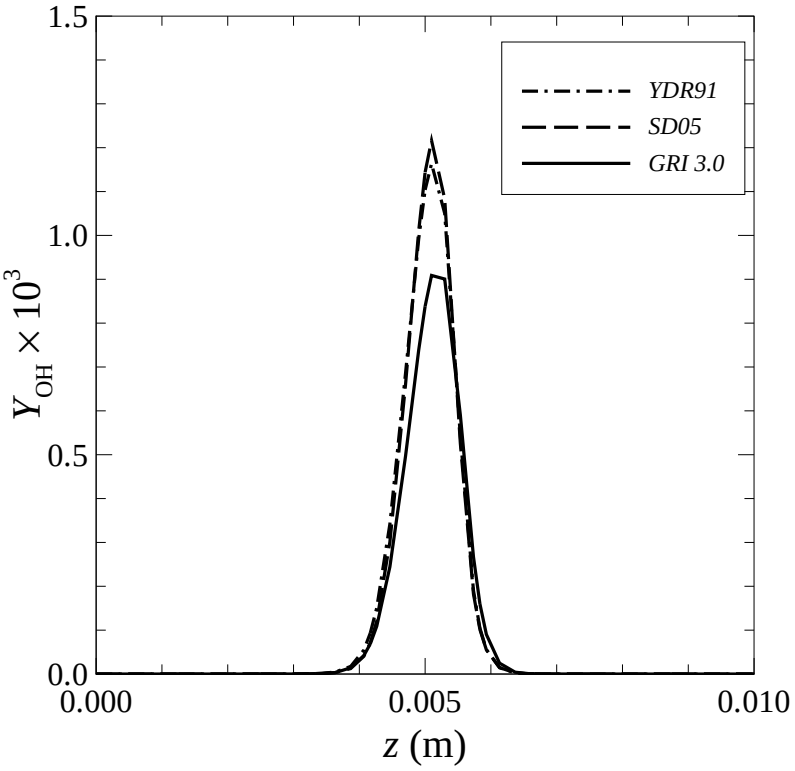

Figure E.1: Comparison of hydroxyl radical mass fraction along the axis between three different hydrogen mechanisms: GRI-Mech 3.0 [H1] (solid line), SD05 [H2] (dashed line), and YDR91 [H4] (dot-dashed line)

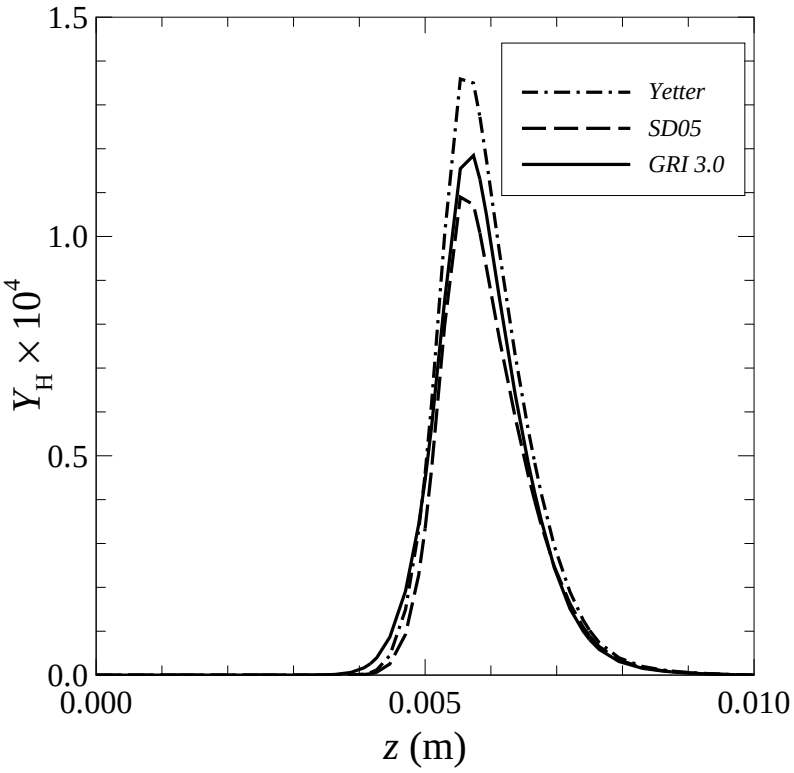

Figure E.2: Comparison of hydrogen radical mass fraction along the axis between three different hydrogen mechanisms. (Legend as in Fig. E.1.)

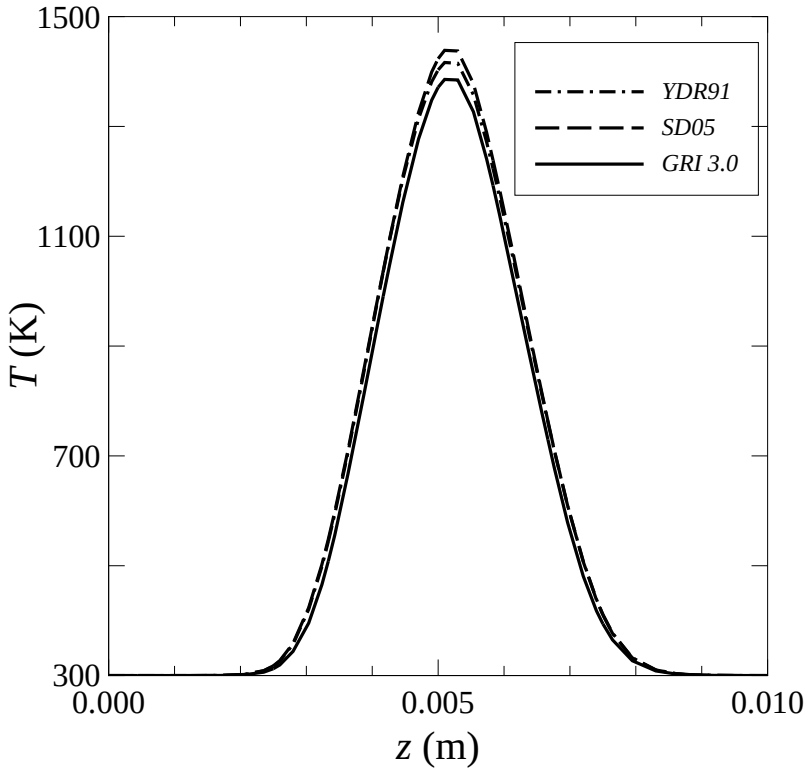

Figure E.3: Comparison of temperature profile along the axis between three different hydrogen mechanisms. (Legend as in Fig. E.1.)

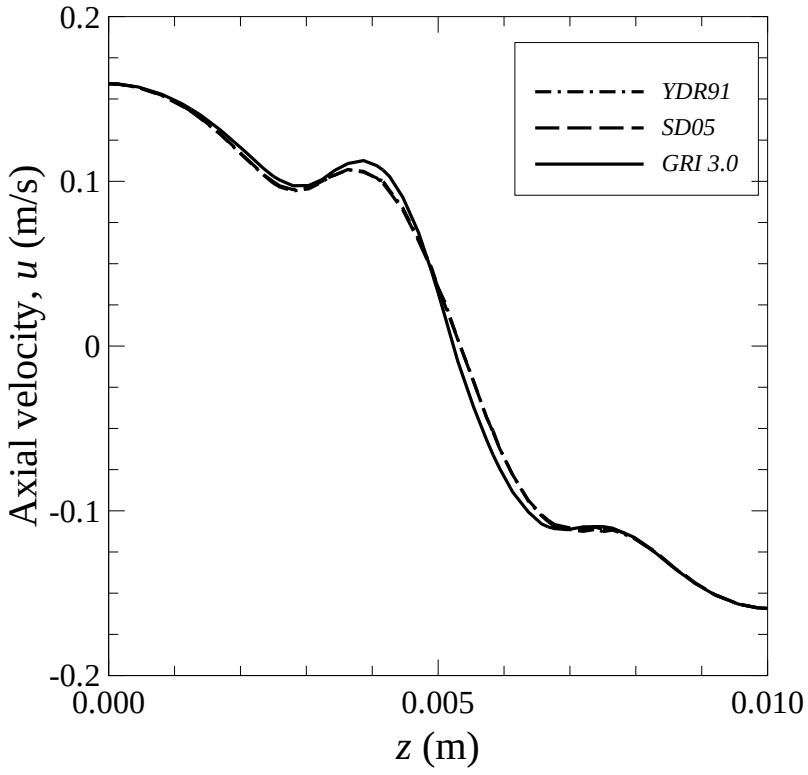

Figure E.4: Comparison of axial velocity profile along the axis between three different hydrogen mechanisms. (Legend as in Fig. E.1.)

Bibliography

Aivazis, M. A. G., April 7-10 2002. Fuego: an extensible toolkit for building chemical kinetics and thermodynamics applications. Presented at Ninth International Conference on Numerical Combustion, Sorrento, Italy. `http://web.ing.unisannio.it/icnc2002/`.

Amsden, A. A., March 1993. KIVA-3: A KIVA Program with Block-Structured Mesh for Complex Geometries. Technical Report LA–12503–MS, Los Alamos National Laboratory.

Amsden, A. A., July 1997. KIVA-3V: A Block-Structured KIVA Program for Engines with Vertical or Canted Valves. Technical Report LA–13313–MS, Los Alamos National Laboratory.

Amsden, A. A., May 1999. KIVA-3V, Release 2, Improvements to KIVA-3V. Technical Report LA–113608–MS, Los Alamos National Laboratory.

Amsden, A. A., O'Rourke, P. J., & Butler, T. D., May 1989. KIVA-II: A Computer Program for Chemically Reactive Flows with Sprays. Technical Report LA–11560–MS, Los Alamos National Laboratory.

Amsden, A. A., Ramshaw, J. D., O'Rourke, P. J., & Dukowicz, J. K., February 1985. KIVA: A Computer Program for Two- and Three-Dimensional Fluid Flows with Chemical Reactions and Fuel Sprays. Technical Report LA–10245–MS, Los Alamos National Laboratory.

Anderson, E., Bai, Z., Bischof, C., Blackford, S., Demmel, J., Dongarra, J., Croz, J. D., Greenbaum, A., Hammarling, S., McKenney, A., & Sorensen, D., 1999. *LAPACK Users' Guide*. SIAM, third edition.

Beizer, B., 1990. *Software Testing Techniques*. International Thomson Computer Press, second edition.

Bell, J. B., Day, M. S., Grcar, J. F., & Lijewski, M. J., 2005a. Stochastic algorithms for the analysis of numerical flame simulations. *Journal of Computational Physics*, **202**: 262–280.

Bell, J. B., Day, M. S., Shepherd, I. G., Johnson, M. R., Cheng, R. K., Grcar, J. F., Beckner, V. E., & Lijews, M. J., 2005b. Numerical simulation of a laboratory-scale turbulent v-flame. *Proceedings of the National Academy of Science of the United States of America*, **102**(29):10006–10011.

Benezech, L. J., Bergthorson, J. M., & Dimotakis, P. E., 2006. Experimental investigation of planar strained methane-air and ethylene-air flames. Technical Report GALCITFM:2006.002, California Institute of Technology. `http://resolver.caltech.edu/CaltechGALCITFM:2006.002`.

Bennett, B. A. V., Fielding, J., Mauro, R. J., Long, M. B., & Smooke, M. D., 1999. A comparison of the structures of lean and rich axisymmetric laminar bunsen flames: application of local rectangular refinement solution-adaptive gridding. *Combustion Theory and Modelling*, **3**(4):657–687.

Bergthorson, J. M., May 2005. *Experiments and Modeling of Impinging Jets and Premixed Hydrocarbon Stagnation Flames*. Ph.D. thesis, California Institute of Technology, Pasadena, CA. `http://resolver.caltech.edu/CaltechETD:etd-05242005-165713`.

Bergthorson, J. M., Sone, K., Mattner, T. W., Dimotakis, P. E., Goodwin, D. G., & Meiron, D. I., 2005a. Impinging laminar jets at moderate reynolds numbers and separation distances. *Physical Review E*, **72**:066307.

Bergthorson, J. M. & Dimotakis, P. E., 2007. Premixed laminar c_1c_2 stagnation flames: Experiments and simulations with detailed thermochemistry models. *Proceedings of the Combustion Institute*, **31**:1139–1147.

Bergthorson, J. M., Goodwin, D. G., & Dimotakis, P. E., 2005b. Particle streak velocimetry and CH laser-induced fluorescence diagnostics in strained, premixed, methaneair flames. *Proceedings of the Combustion Institute*, **30**:1637–1644.

Bird, R. B., Stewart, W. E., & Lightfoot, E. N., 2002. *Transport Phenomena*. J. Wiley, New York.

Blackburn, H. M. & Henderson, R. D., 1999. A study of two-dimensional flow past an oscillating cylinder. *Journal of Fluid Mechanics*, **385**:255–286.

Blackburn, H. M. & Lopez, J. M., 2002. Modulated rotating waves in an enclosed swirling flow. *Journal of Fluid Mechanics*, **465**:33–58.

Blackburn, H. M. & Sherwin, S. J., 2004. Formulation of a Galerkin spectral element-Fourier method for three-dimensional incompressible flows in cylindrical geometries. *Journal of Computational Physics*, **197**:759–778.

Blackford, L. S., Choi, J., Cleary, A., D'Azevedo, E., Demmel, J., Dhillon, I., Dongarra, J., Hammarling, S., Henry, G., Petitet, A., Stanley, K., Walker, D., & Whaley, R. C., 1997. *ScaLAPACK Users' Guide*. SIAM.

Boyd, J. P., 2000. *Chebyshev and Fourier spectral methods*. Dover Publications, Inc., Mineola, NY, second edition.

Bradley, D., Gaskell, P. H., & Gu, X. J., 1996. Burning velocities, markstein lengths, and flame quenching for spherical methane-air flames: A computational study. *Combustion and Flame*, **104**:176–198.

Buckmaster, J. D. & Ludford, G. S. S., 1982. *Theory of laminar flames*. Cambridge University Press.

Candel, S. M. & Poinsot, T. J., 1990. Flame stretch and the balance equation for the flame area. *Combustion Science and Technology*, **70**:1–15.

Celik, I., Yavuz, I., Smirnov, A., Smith, J., Amin, E., & Gel, A., 2000. Prediction of in-cylinder turbulence for IC engines. *Combustion Science and Technology*, **153**:339–368.

Chung, S. H. & Law, C. K., 1984. An invariant derivation of flame stretch. *Combustion and Flame*, **55**:123–125.

Clavin, P. & Joulin, G., 1983. Premixed flames in large scale and high intensity turbulent flow. *Le Journal De Physique—Letters*, **44**:L–1–L–12.

Coffee, T. & Heimerl, J., 1981. Transport algorithms for premixed, laminar steady-state flames. *Combustion and Flame*, **43**:273–289.

Cohen, S. D. & Hindmarsh, A. C., September 1994. CVODE user guide. Technical Report LLNL Report UCRL-MA-118618, Lawrence Livermore National Laboratory.

Curtiss, C. F. & Bird, R. B., 1999. Multicomponent diffusion. *Industrial & Engineering Chemistry Research*, **38**:2515–2522.

Davis, S. G., Quinard, J., & Searby, 2001. A numerical investigation of stretch effects in counterflow, premixed laminar flames. *Combustion Theory and Modeling*, **5**:353–362.

Davis, S. G., Quinard, J., & Searby, 2002a. Determination of Markstein numbers in counterflow premixed flames. *Combustion and Flame*, **130**:112–122.

Davis, S. G., Quinard, J., & Searby, 2002b. Markstein numbers in counterflow, methane- and propane- air flames: A computational study. *Combustion and Flame*, **130**:123–136.

Davis, S., Law, C., & Wang, H., 1999. Propene pyrolysis and oxidation kinetics in a flow reactor and laminar flames. *Combustion and Flame*, **119**:375–399.

Day, M. S. & Bell, J. B., 2000. Numerical simulation of laminar reacting flows with complex chemistry. *Combustion Theory and Modelling*, **4**(4):535–556.

Denbigh, K., 1955. *The principles of chemical equilibrium, with applications in chemistry and chemical engineering*. Cambridge University Press.

Deshaies, B. & Cambray, P., 1990. The velocity of a premixed flame as a function of the flame stretch: An experimental study. *Combustion and Flame*, **82**:361–375.

Deshpande, M. D. & Vaishnav, R. N., 1982. Submerged laminar jet impingement on a plane. *Journal of Fluid Mechanics*, **114**:213–236.

Deville, M. O., Fischer, P. F., & Mund, E. H., 2002. *High-Order Methods for Incompressible Fluid Flow*. Cambridge University Press.

Dimotakis, P. E., 2005. Turbulent mixing. *Annual Review of Fluid Mechanics*, **37**:329–356.

Dong, Y., Vagelopoulos, C. M., Spedding, G. R., & Egolfopoulos, F. N., 2002. Measurement of laminar flame speeds through digital particle image velocimetry: Mixtures of methane and ethane with hydrogen, oxygen, nitrogen, and helium. *Twenty-Nineth Symposium (International) on Combustion*, **29**:1419–1426.

Dowd, K. & Severance, C., 1998. *High Performance Computing*. O'Reilly & Associates, Inc., second edition.

Egolfopoulos, F. N., 1994. Geometric and radiation effects on steady and unsteady strained laminar flames. *Twenty-Fifth Symposium (International) on Combustion*, pages 1375–1381.

Egolfopoulos, F. N. & Dimotakis, P. E., 2001. A comparative numerical study of premixed and non-premixed ethylene flames. *Combustion Science and Technology*, **162**: 19–35.

Egolfopoulos, F. N., Du, D. X., & Law, C. K., 1992. A comprehensive study of methanol kinetics in freely-propagating and burner-stabilized flames, flow and static reactors, and shock-tubes. *Combustion Science and Technology*, **83**:33–75.

Egolfopoulos, F. N., Zhang, H., & Zhang, Z., 1997. Wall effects on the propagation and extinction of steady, strained, laminar premixed flames. *Combustion and Flame*, **109**:237–252.

H. W. Emmons (Ed.), 1958. *Fundamentals of gas dynamics*. Princeton University Press.

Ern, A. & Giovangigli, V., 1994. *Multicomponent transport algorithms*. Springer-Verlag.

Ern, A. & Giovangigli, V., 1998. Thermal diffusion effects in hydrogen-air and methane-air flames. *Combustion Theory and Modelling*, **2**(4):349–372.

Ern, A. & Giovangigli, V., 1999. Impact of detailed multicomponent transport on planar and counterflow hydrogen/air and methane/air flames. *Combustion Science and Technology*, **149**:157–181.

Fischer, P. F., Ho, L.-W., Karniadakis, G. E., Rønquist, E. M., & Patera, A. T., 1988. Recent advances in parallel spectral element simulation of unsteady tncompressible flows. *Computers & Structures*, **30**:217–231.

Fischer, P. F. & Patera, A. T., 1991. Parallel spectral element solution of the stokes problem. *Journal of Computational Physics*, **92**:380–421.

Fischer, P. F. & Rønquist, E. M., 1994. Spectral element methods for large scale parallel navier-stokes calculations. *Computer methods in applied mechanics and engineering*, **116**:69–76.

Frenklach, M., Wang, H., & Rabinowitz, M. J., 1992. Optimization and analysis of large chemical kinetic mechanisms using the solution mapping method – combustion of methane. *Progress in Energy and Combustion Science*, **18**:47–73.

Frouzakis, C. E., Lee, J., Tomboulides, A. G., & Boulouchos, K., 1998. Two-dimensional direct numerical simulation of opposed-jet hydrogen-air diffusion flame. *Twenty-Seventh Symposium (International) on Combustion*, pages 571–577.

Gamma, E., Helm, R., Johnson, R., & Vlissides, J., 1994. *Design Patterns*. Addison-Wesley Publishing Company.

Glarborg, P., Kristensen, P. G., Dam-Johansen, K., Alzueta, M. U., Millera, A., & Bilbao, R., 2000. Nitric oxide reduction by nonhydrocarbon fuels. implications for reburning with gasification gases. *Energy & Fuels*, **14**:828–838.

Goodwin, D. G., 2003. An open-source, extensible software suite for CVD process simulation. In M. D. Allendorf, F. Maury, & F. Teyssandier (Eds.), *Proceedings of CVD XVI and EuroCVD Fourteen,* Electrochemical Society, pages 155–162.

Gray, A., 1997. *Modern Differential Geometry of Curves and Surfaces with Mathematica*. CRC Press, second edition.

Gresho, P. M., 1991. Incompressible fluid dynamics: some fundamental formulation issues. *Annual Review of Fluid Mechanics*, **23**:413–453.

Gropp, W., Keyes, D., McInnes, L. C., & Tidriri, M. D., 2000. Globalized Newton-Krylov-Schwarz algorithms and software for parallel implicit CFD. *The International Journal of High Performance Computing Applications*, **14**:102–136.

Gropp, W., Lusk, E., & Skjellum, A., 1994. *Using MPI : portable parallel programming with the message-passing interface*. MIT Press.

Gropp, W., Lusk, E., & Skjellum, A., 1999. *Using MPI-2 : advanced features of the message-passing interface*. MIT Press.

Han, Z. & Reitz, R. D., 1995. Turbulence modeling of internal combustion engines using RNG $k - \varepsilon$ models. *Combustion Science and Technology*, **106**:267–295.

Haworth, D. C. & Jansen, K., 2000. Large-eddy simulation on unstructured deforming meshes: towards reciprocating ic engines. *Computers and Fluids*, **29**:493–524.

Henderson, R. D., 1999a. Adaptive spectral element methods for turbulence and transition, In: *High-order methods for computational physics*, T. Barth & H. Deconinck (Eds.), pages 225–324, Springer-Verlag. Lecture notes in computational science and engineering 9.

Henderson, R. D., 1999b. Dynamic refinement algorithms for spectral element methods. *Computer methods in applied mechanics and engineering*, **175**:395–411.

Henderson, R. D. & Barkley, D., 1996. Secondary instability in the wake of a circular cylinder. *Physics of Fluids*, **8**(6):1683–1685.

Henderson, R. D. & Karniadakis, G. E., 1995. Unstructured spectral element methods for simulation of turbulent flows. *Journal of Computational Physics*, **122**:191–217.

Hirasawa, T., Sung, C. J., Joshi, A., Yang, Z., Wang, H., & Law, C. K., 2002. Determination of laminar flame speeds using digital particle image velocimetry: Binary fuel blends of ethylene, n-butane, and toluene. *Twenty-Nineth Symposium (International) on Combustion*, **29**:1427–1434.

Hirschfelder, J. O., Curtiss, C. F., & Bird, R. B., 1954. *Molecular Theory of Gases and Liquids*. Wiley, New York.

Hung, P., May 2003. *Algorithms for Reaction Mechanism Reduction and Numerical Simulation of Detonations Initiated by Projectiles*. Ph.D. thesis, California Institute of Technology, Pasadena, CA.

Ianenko, N. N., 1971. *The method of fractional steps*. Springer-Verlag.

Karniadakis, G. E., Israeli, M., & Orszag, S., 1991. High-order splitting methods for the incompressible Navier-Stokes equations. *Journal of Computational Physics*, **97**: 414–443.

Karniadakis, G. E. & Sherwin, S. J., 1999. *Spectral/hp element methods for CFD*. Oxford University Press, New York, NY.

Kee, R. J., Coltrin, M. E., & Glarborg, P., 2003. *Chemically Reacting Flow—Theory & Practice*. John Wiley & Sons, Inc., New Jersey.

Kee, R. J., Dixon-Lewis, G., Warnatz, J., Coltrin, M. E., Miller, J. A., & Moffat, H. K., 1986. Transport: A software package for the evaluation of gas-phase, multicomponent transport properties. Technical Report SAND86-8246B, Sandia National Laboratory.

Kee, R. J., Miller, J. A., Evans, G. H., & Dixon-Lewis, G., 1988. A computational model of the structure and extinction of strained, opposed flow, premixed methane-air flames. *Twenty-Second Symposium (International) on Combustion*, pages 1479–1494.

Kim, W.-W., Menon, S., & Mongia, H. C., 1999. Numerical simulations of reacting flows in a gas turbine combustor. *Combustion Science and Technology*, **143**:25–62.

Knupp, P. & Salari, K., 2003. *Verification of Computer Codes in Computational Science and Engineering*. Chapman & Hall.

Kostiuk, L. W., Bray, K. N. C., & Cheng, R. K., 1993. Experimental study of premixed turbulent combustion in opposed streams: Part I — non-reacting flow field. *Combustion and Flame*, **92**:377–395.

Kovasznay, L. I. G., 1948. Laminar flow behind a two-dimensional grid. *Proceedings of the Cambridge Philosophical Society*, **44**:58–62.

Lagerstrom, P., 1964. *Laminar flow theory*. Princeton University Press.

Lakos, J., 1996. *Large-Scale C++ Software Design*. Addison-Wesley Publishing Company.

Landau, L. D., 1944. On the theory of slow combustion. *Acta Physicochimica*, **19**:77.

Lange, T., February 19-23 2007. Will pringles fly? how P&G is using modeling & simulation to innovate innovation. Presented at SIAM Conference on Computational Science & Engineering, Costa Mesa, California. `http://www.siam.org/meetings/cse07/`.

Law, C. K., 1988. Dynamics of stretched flames. *Twenty-Second Symposium (International) on Combustion*, pages 1381–1402.

Law, C. K. & Sung, C. J., 2000. Structure, aerodynamics, and geometry of premixed flamelets. *Progress in Energy and Combustion Science*, **26**:459–505.

Leonard, A. & Wray, A., 1982. A new numerical method for the simulation of three-dimensional flow in a pipe, In *Lecture Notes in Physics, No. 170: Eighth international conference on numerical methods in fluid dynamics*, pages 335–342, Springer-Verlag.

Maas, U. & Warnatz, J., 1988. Ignition process in hydrogen-oxygen mixtures. *Combustion and Flame*, **74**:53–69.

Majda, A. & Sethian, J. A., 1985. The derivation and numerical solution of the equations for zero mach number combustion. *Combustion Science and Technology*, **42**:185–205.

Marinov, N. M., 1999. A detailed chemical kinetic model for high temperature ethanol oxidation. *International Journal of Chemical Kinetics*, **31**(3):183–220.

Markstein, G. H., 1951. Experimental and theoretical studies of flame-front stability. *Journal of the Aeronautical Sciences*, **18**:199–209.

Markstein, G. H., 1964. *Nonsteady Flame Propagation.* Pergamon Press, Oxford.

Matalon, M. & Matkowsky, B. J., 1982. Flames as gasdynamic discontinuities. *Journal of Fluid Mechanics*, **124**:239–259.

Mathur, S., Tondon, P. K., & Saxena, S. C., 1967. Thermal conductivity of binary ternary and quaternary mixtures of rare gases. *Molecular Physics*, **12**:569.

Matsushima, T. & Marcus, P. S., 1995. A spectral method for polar coordinates. *Journal of Computational Physics*, **120**:365–374.

McKee, B., June 2004. The pool gets cooler. *I.D.*, pages 78–81.

McMurtry, P. A., Jou, W.-H., Riley, J. J., & Metcalfe, R. W., 1986. Direct numerical simulations of a reacting mixing layer with chemical heat release. *AIAA Journal*, **24**(6):962–970.

Mendes-Lopes, J. M. C. & Daneshyar, H., 1985. Influence of strain fields on flame propagation. *Combustion and Flame*, **60**:29.

Miles, R. & Hamilton, K., 2006. *Learning UML 2.0*. O'Reilly & Associates, Inc.

Mohseni, K. & Colonius, T., 2000. Numerical treatment of polar coordinate singularities. *Journal of Computational Physics*, **157**:787–795.

Monchick, L. & Mason, E. A., 1961. Transport properties of polar gases. *Journal of Chemical Physics*, **35**(5):1676.

Najm, H. N. & Knio, O. M., 2005. Modeling low mach number reacting flow with detailed chemistry and transport. *Journal of Scientific Computing*, **25**:263–287.

Ortega, J. M., 1990. *Numerical Analysis A Second Course*. SIAM.

Patera, A. T., 1984. A spectral element method for fluid dynamics: Laminar flow in a channel expansion. *Journal of Computational Physics*, **54**:468–488.

Pellet, G. L., Isssac, K. M., Humphreys, W. M., Jr., Gartrell, L. R., Roberts, W. L., Dancey, C. L., & Northam, G. B., 1998. Velocity and thermal structure, and strain-induced extinction of 14 to 100% hydrogen-air counterflow diffusion flames. *Combustion and Flame*, **112**:575–592.

Pelletier, D., Turgeon, E., & Tremblay, D., 2004. Verification and validation of impinging round jet simulations using an adaptive FEM. *International journal for numerical methods in fluids*, **44**(7):737–763.

Ramshaw, J. D., O'Rourke, P. J., & Stein, L. R., 1985. Pressure-gradient scaling method for fluid-flow with nearly uniform pressure. *Journal of Computational Physics*, **58**:361–376.

Roy, C. J., 2005. Review of code and solution verification procedures for computational simulation. *Journal of Computational Physics*, **205**:131–156.

San Diego mechanism. *Chemical-Kinetic Mechanisms for Combustion Applications*, Center for Energy Research, University of California at San Diego, 2005. `http://maeweb.ucsd.edu/combustion/cermech`.

Schlichting, H., 1960. *Boundary Layer Theory*. McGraw-Hill, Inc., New York.

Shirouzu, N., 2006. Toyota review reveals need for more quality checks. *The Wall Street Journal*, (December 11):B3D.

Smith, G. P., Golden, D. M., Frenklach, M., Moriarty, N. W., Eiteneer, B., Goldenberg, M., Bowman, C. T., Hanson, R. K., Song, S., Gardiner, J., W. C., Lissianski, V. V., & Qin, Z. GRI-Mech 3.0. `http://www.me.berkeley.edu/gri_mech/`.

Smooke, M. D., Puri, I. K., & Seshadri, K., 1986. A comparison between numerical calculations and experimental measurements of the structure of a counterflow diffusion flame burning diluted methane in diluted air. *Twenty-First Symposium (International) on Combustion*, **21**:1783–1792.

Smooke, M. D., Xu, Y., Zurn, R. M., Lin, P., Frank, J. H., & Long, M. B., 1992. Computational and experimental study of oh and ch radicals in axisymmetric laminar diffusion flames. *Twenty-Fourth Symposium (International) on Combustion*, pages 813–821.

Sone, K. & Menon, S., 2003. Effect of subgrid modeling on the in-cylinder unsteady mixing process in a direct injection engine. *Journal of Engineering for Gas Turbines and Power*, **125**:435–443.

Stroustrup, B., 1991. *The C++ PROGRAMMING LANGUAGE*. Addison-Wesley Publishing Company, second edition.

Tan, Y., Dagaut, P., Cathonnet, M., Boettner, J. C., Bachman, J. S., & Carlier, P., 1994. Natural gas and blends oxidation and ignition: Experiments and modeling. *Twenty-Fifth Symposium (International) on Combustion*, **25**:1563–1569.

Tien, J. H. & Matalon, M., 1991. On the burning velocity of stretched flames. *Combustion and Flame*, **84**:238–248.

Tomboulides, A. G., Lee, J. C. Y., & Orszag, S. A., 1997. Numerical simulation of low mach number reactive flows. *Journal of Scientific Computing*, **12**(2):139–167.

Tomboulides, A. G. & Orszag, S. A., 1998. A quasi-two-dimensional benchmark problem for low mach number compressible codes. *Journal of Computational Physics*, **146**: 691–706.

Tomboulides, A. G. & Orszag, S. A., 2000. Numerical investigation of transitional and weak turbulent flow past a sphere. *Journal of Fluid Mechanics*, **416**:45–73.

Turányi, T., Zalotai, L., Dóbé, S., & Bérces, T., 2002. Effect of the uncertainty of kinetic and thermodynamic data on methane flame simulation results. *Physical Chemistry Chemical Physics*, **4**:2568–2578.

Turns, S. R., 2000. *An Introduction to Combustion*. McGraw-Hill Inc.

Vagelopoulos, C. M. & Egolfopoulos, F. N., 1998. Direct experimental determination of laminar flame speeds. *Twenty-Seventh Symposium (International) on Combustion*, pages 513–519.

Wang, H. & Frenklach, M., 1997. A detailed kinetic modeling study of aromatics formation in laminar premixed acetylene and ethylene flames. *Combustion and Flame*, **110**:173–221.

Wang, H., Laskin, A., Djurisic, Z. M., Law, C. K., Davis, S. G., & Zhu, D. L., 1999. A comprehensive mechanism of C_2H_x and C_3H_x fuel combustion. *the 1999 Fall Technical Meeting of the Eastern States Section of the Combustion Institute, Raleigh, NC*, pages 129–132.

Westbrook, C. K. & Dryer, F. L., 1981. Simplified reaction mechanisms for the oxidatioin of hydrocarbon fuels in flames. *Combustion Science and Technology*, **27**:31–43.

Williams, F. A., 1975. Recent advances in theoretical descriptions of turbulent diffusion flames, In: *Turbulent Mixing in Nonreactive and Reactive Flows*, S. N. B. Murthy (Ed.), pages 189–208.

Williams, F. A., 1985. *Combustion Theory*. Addison-Wesley Publishing Company, Redwood City, CA, second edition.

Williams, F. A., 2000. Progress in knowledge of flamelet structure and extinction. *Progress in Energy and Combustion Science*, **26**:657–682.

Wu, C. & Law, C., 1984. On the determination of laminar flame speeds from stretched flames. *Twentieth Symposium (International) on Combustion*, pages 1941–1949.

Yetter, R. A., Dryer, F. L., & Rabitz, H., 1991. A comprehensive reaction-mechanism for carbon-monoxide hydrogen oxygen kinetics. *Combustion Science and Technology*, **79**: 97–128.